Digital Chemical Engineering 6 (2023) 100081

Contents lists available at ScienceDirect

Digital Chemical Engineering

journal homepage: www.elsevier.com/locate/dche

Best practices and methods

Model-based design and optimization of GSSR chromatography for peptide purification

Tiago P.D. Santos [a], Rita P. Fernandes [b], Rui P.P.L. Ribeiro [a], Cristina Peixoto [b], José P.B. Mota [a,*]

[a] LAQV-REQUIMTE, Departamento de Química, NOVA School of Science and Technology, FCT NOVA, 2829-516 Caparica, Portugal
[b] IBET – Instituto de Biologia Experimental e Tecnológica, Apartado 12, 2780-901 Oeiras, Portugal

ARTICLE INFO

Keywords:
Multicolumn chromatography
Solvent gradient
GSSR process
Process optimization
Interior point method
Optimization under uncertainty

ABSTRACT

Gradient with Steady State Recycle (GSSR) is a recently developed process for center-cut separation by solvent-gradient chromatography. The process comprises a multicolumn, open-loop system with cyclic steady-state operation that simulates a solvent gradient moving countercurrently with respect to the solid phase. However, the feed is always injected into the same column and the product always collected from the same column as in single-column batch chromatography. Here, three-column GSSR chromatography for peptide purification is optimized using state-of-the-art mathematical programming tools. The optimization problem is formulated using a full-discretization approach for steady periodic dynamics. The resulting nonlinear programming problem is solved by an efficient open-source interior-point solver coupled to a high-performance parallel linear solver for sparse symmetric indefinite matrices. The procedure is successfully employed to find optimal solutions for a series of process design problems with increasing number of decision variables. In addition to productivity and recovery, process performance is analyzed in terms of two key performance indicators: dilution ratio and solvent consumption ratio. Finally, the problem of robust process design under uncertainty in the solvent gradient manipulation is examined. The best solution is chosen only among candidate solutions that are robust feasible, i.e., remain feasible for all modifier gradient perturbations within the accuracy range of the gradient pump. This gives rise to a robust approach to optimal design in which the nominal problem is replaced by a worst case problem. Overall, our work illustrates the advantages of using advanced mathematical programming tools in designing and optimizing a GSSR process for which it is difficult to deduce sufficiently general heuristic design rules.

1. Introduction

Chromatography is one of the most expensive steps in the downstream processing platform for the purification of a biopharmaceutical product, one reason being that many chromatographic processes are still run in batch mode. Single-column batch chromatography (SCBC) is simple to implement and can achieve high purity, but at the cost of decreased yield as well as increased solvent consumption (Baur et al., 2016). In SCBC the product and waste cuts are collected at the downstream end of the column but at different times. Therefore, time (or elution volume) is the only manipulated variable with which to define the fractional cuts. Furthermore, a solvent gradient can only be introduced at the upstream end of the system. This does not allow much flexibility to dynamically adjust the solvent composition profile along the length of the chromatographic medium. Although packing the stationary phase into a single column works well for many binary separations, this seems to be overly restrictive for center-cut separation—one in which the target product is contained in the intermediate of three main fractions or cuts.

Continuous multi-column chromatography, on the other hand, while having the disadvantage of a higher initial investment cost, achieves the same purity level, without loss of yield or increased solvent consumption, by internally recirculating the impure product fractions and excess solvent (De Luca et al., 2020; Mahajan et al., 2012; Warikoo et al., 2012). This is due to the extra degrees of freedom arising from the division of the stationary phase into a circular train of columns, which makes the manipulation of the cuts and generation of the solvent gradient much more flexible; moreover, with such a column arrangement some of the cuts can be recirculated from the downstream end of the system to its upstream end in an open-loop configuration.

Several continuous multicolumn processes have been developed over the past two decades to overcome the disadvantages of traditional

* Corresponding author.
E-mail address: pmota@fct.unl.pt (J.P.B. Mota).

https://doi.org/10.1016/j.dche.2022.100081
Received 16 October 2022; Received in revised form 20 November 2022; Accepted 19 December 2022
Available online 28 December 2022

Abbreviations

3C-PCC	three-column Periodic Counter Current
AMPL	Algebraic Mathematical Programming Language
BLAS	Basic Linear Algebra Subroutines
CSS	cyclic steady state
DANLP	differential–algebraic nonlinear programming
EtOH	ethanol
GSSR	Gradient with Steady State Recycle (GSSR)
LAPACK	Linear Algebra PACKage
MCSGP	Multicolumn Countercurrent Solvent Gradient Process
NLP	nonlinear programming
SCBC	single-column batch chromatography
SMCC	Sequential Multicolumn Chromatography
SW	switch interval
TFA	terephthalic acid
UV	ultraviolet
WSMP	Watson Sparse Matrix Package

SCBC, including VARICOL (Ludemann-Hombourger et al., 2000), Sequential Multicolumn Chromatography (SMCC) (Holzer et al., 2008), Multicolumn Countercurrent Solvent Gradient Process (MCSGP) (Ströhlein et al., 2006; Aumann and Morbidelli, 2007; Aumann et al., 2007; Aumann and Morbidelli, 2008; Müller-Späth et al., 2008; Steinebach et al., 2017), Gradient with Steady State Recycle (GSSR) (Silva et al., 2010), CaptureSMB (Angarita et al., 2015), and Multicolumn Periodic Counter Current (3C-PCC) chromatography (Godawat et al., 2012; Kumar and Rathore, 2014; Brämer et al., 2019), among others (Lee, 2020; Hur and Wankat, 2005; Silva et al., 2012). All these processes have been proven to achieve high purity while maintaining high yield and reducing solvent consumption by significant margins (Challener, 2018).

Although continuous chromatography is in theory better than SCBC, this certainly does not mean that the former does not have its risks. The biggest of these is the infrastructure already in place. If the downstream process platform uses at least one batch step for purification, switching everything to a continuous process may not be cost effective (Gomis-Fons et al., 2020; Pollock et al., 2017). Furthermore, since continuous multicolumn chromatography potentially has a large number of degrees of freedom, it may require extensive optimization for each process type and application. As an example, if the mixture to be separated or resin or mobile phase are changed, the process optimization has to be redone from scratch, which can take considerable time (Shi et al., 2020).

Here we focus on the model-based design and optimization of three-column GSSR chromatography (Silva et al., 2010) and show how its performance can be significantly improved using state-of-the-art nonlinear mathematical programming. We highlight the advantages of using advanced optimization tools to design and optimize a process for which it is difficult to deduce sufficiently general heuristic design rules. The aim of this work is not only to maximize the process throughput but also to explore the possibility of reducing the solvent consumption, increasing product concentration and, if possible, reducing the number of steps of the operating cycle.

Past studies on model-based optimization for single- and multi-column chromatographic processes were reviewed by Kawajiri (2021), with focus placed on applications of mathematical programming techniques. Lin et al. (2021) have also recently reviewed model-assisted approaches and their applications in continuous chromatography process development, validation, and control. Schmölder and Kaspereit (2020) introduced a modular framework for the modeling and optimization of advanced chromatographic processes. Others have provided examples of the benefits of increased productivity and cost savings obtained from using optimized continuous multicolumn chromatography (Sreedhar and Kawajiri, 2014; Pagkaliwangan et al., 2019).

Our paper is structured as follows. First, the GSSR process is described and the case study of three-column GSSR chromatography for peptide purification is presented. The GSSR cycle is designed and its operating conditions optimized using state-of-the-art, model-based mathematical programming. After the description of the process model, adopted solution procedure, and numerical implementation, the process is subjected to a series of optimizations with increasing number of decision variables. It is shown that the optimization effort is offset by a significant increase in process performance over previous heuristically determined operating conditions (Silva et al., 2010). The modifier gradient slope in solvent A is one of the operating parameters to which purity and recovery are most sensitive. Two examples are presented of how to robustly design the operating conditions under uncertainty of experimentally realizing the said gradient. The paper ends with some brief conclusions and perspectives for future work. Section 1 of the Supporting Information (SI) file contains a full list of symbols and their meanings.

2. Process description

The GSSR process (Silva et al., 2010) comprises a multi-column, open-loop system with cyclic steady-state operation that simulates a solvent gradient moving countercurrently with respect to the solid phase. The process superimposes three periodic events applied to a ring of chromatographic columns in an open-loop configuration: (i) a moving solvent gradient, (ii) feed injection at a fixed point in the system, and (iii) product collection at a fixed point in the system.

Although GSSR chromatography can be implemented with a plurality of columns, we focus our attention on the three-column configuration, as it is the one that uses the least number of columns for solving the generic center-cut separation problem. One such system was successfully used by us for peptide purification (Silva et al., 2010). In the most generic scenario the three-column train is fed with three different solvents: solvent A, whose composition can be changed linearly in time, and two isocratic solvents, B and C. Optionally, a fourth solvent can replace solvent C during certain fractions of the cycle to implement a desorption zone for in-line regeneration or cleaning in place.

Whichever the case, the operating cycle is divided into a number of uniform switch intervals equal to the number of columns (in the present case, three). The inlet positions and flow rates of the solvent streams are defined for a single switch interval as a set of steps over that time interval. The sequence is then repeated a number of times equal to the number of columns. The only difference between one switch interval and the next is the switching of the solvent inlets and open outlets by one column in the direction of the fluid flow. This procedure simulates the counter-current contact between the moving solvent gradient and the solid phase.

Fig. 1 shows the step sequence of the solvent lines for a full cycle where, without any loss of generality, it is assumed that the cycle starts with solvent A being injected into the leftmost column. The positions of the solvent inlets are periodic in time, with period τ, where τ is the duration of the switch interval. There is always an open outlet, which is taken as a waste fraction, to keep the system in open loop. The net effect of this cyclic scheme is to simulate the counter-current motion of the solid phase with respect to an open-loop solvent gradient that is τ-periodic in time. The duration of the overall cycle is $t_{\mathrm{cyc}} = N_{\mathrm{c}}\tau$, where N_{c} is the number of columns.

As noted above, two additional steps complete the design of a GSSR cycle: (i) the time interval during which fresh feed is supplied to the process; and (ii) the time interval during which the purified product is collected. These two steps take place only once per cycle and,

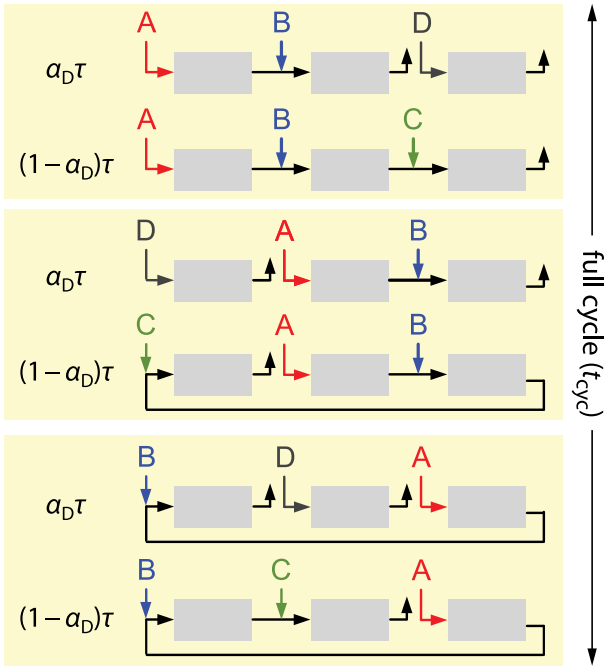

Fig. 1. Basic sequence of the solvent lines for a three-column GSSR process. Solvent D can be used to implement a desorption zone for in-line regeneration or cleaning in place. In this case, during an initial fraction, say $0 < \alpha_D < 1$, of the switch interval, the most downstream column is disconnected and eluted with solvent D. During the remaining $1-\alpha_D$ fraction of the switch interval the process operates with all columns connected in an open-loop configuration. All active outlets are diverted to waste. The duration of the overall cycle is $t_{cyc} = N_c\tau$, where N_c is the number of columns and τ the duration of the switch interval.

depending on the difficulty of the chromatographic separation, they can be performed at different intervals of the cycle, or take place at the same time, or partially overlap. However, the feed is always injected into the same column as a rectangular pulse and the product is always collected from the same column. As discussed next, it is convenient that the feed injection and product collection take place at opposite ends of the column train in order to set the longest path between the feed inlet and the product outlet.

If the unit is operated near its maximum throughput, the target solute reaches the collection point at the downstream end of the column train partially mixed with its two nearest neighboring impurities. In order to avoid penalizing the recovery, the two impure cuts surrounding the purified product—each containing one edge of the product concentration profile—must be recirculated to the feed point at the upstream end of the system. For optimal performance, the two mixed cuts should be recirculated by encircling the feed pulse loaded into the feed column. Therefore, for difficult separations that require this recycling strategy the feed and product withdrawal steps must overlap in time. Thus, the feed step must occur when the eluate is recirculated from the downstream end of the column train to the feed point at the upstream end. Potential candidates for this purpose are any of the last three steps in Fig. 1.

Fig. 2 shows examples of cases where the feed injection and product collection take place at opposite ends of the column train. From a process systems engineering point of view, we consider the ensemble of configurations shows in Figs. 1 and 2 as a superstructure from which optimal cycles can be extracted for a particular separation. Experience has shown that to get the most efficient separation the feed pulse should be moved through the system by the moving solvent gradient (A) and not eluted isocratically with either solvent B or C. Hence, feeding and collecting the product during the third switch interval is the most likely option.

3. Case study

We use as a case study the purification of a crude peptide mixture by reversed-phase liquid chromatography (RPLC) reported previously by us (Silva et al., 2010). RPLC is widely used in the purification of peptides for pharmaceutical formulations, due to its ability to provide high-resolution separation combined with good reproducibility. However, peptide mixtures can be complex, with significantly heterogeneous physical chemistries (including hydrophobic and highly hydrophilic compounds), thus rendering their efficient separation by RPLC challenging (Abbood et al., 2009).

The packing material is Kromasil C18 (Eka Chemicals AB, Sweden) and the mobile phase an aqueous solution of ethanol (EtOH) with a fixed residual amount (0.1% v/v) of terephthalic acid (TFA); the EtOH concentration is allowed to vary between 0.25 and 0.5 v/v. The retention behavior of the crude peptide mixture was analyzed at analytical scale on 5 μm Kromasil C18, purchased prepacked into a 0.46 cm × 15 cm column (Fig. 3). The GSSR process was designed and optimized to use 25 μm Kromasil C18 packed into three 1 cm × 10 cm stainless steel columns.

The analytical chromatogram in Fig. 3 shows that the crude mixture is characterized by three main cuts: a weakly adsorbing (early eluting) cut containing three major impurities, an intermediate cut with the target product and at least four neighboring impurities, and a strongly adsorbing (late eluting) cut containing three impurities. The target product corresponds to the largest peak of the chromatogram, with roughly 50% of the total peak area.

The adsorption equilibrium of the competing solutes is the basis for the design or optimization of any chromatographic process governed by adsorption thermodynamics; this is the case for the peptide mixture on the 25 μm Kromasil C18 phase for the working range of linear velocities used at preparative or production scale. Although mass transfer and axial dispersion smooth the concentration profiles, they do not change their stoichiometric positions when the process is not limited by adsorption kinetics.

As shown by Silva et al. (2010), the adsorption behavior of the feed mixture is strongly dependent on the EtOH concentration (c_0) in the mobile phase. The solutes are assumed to be linearly adsorbed since they are in dilute concentration in the feed. When dealing with the purification of a complex, multicomponent mixture, like the crude peptide

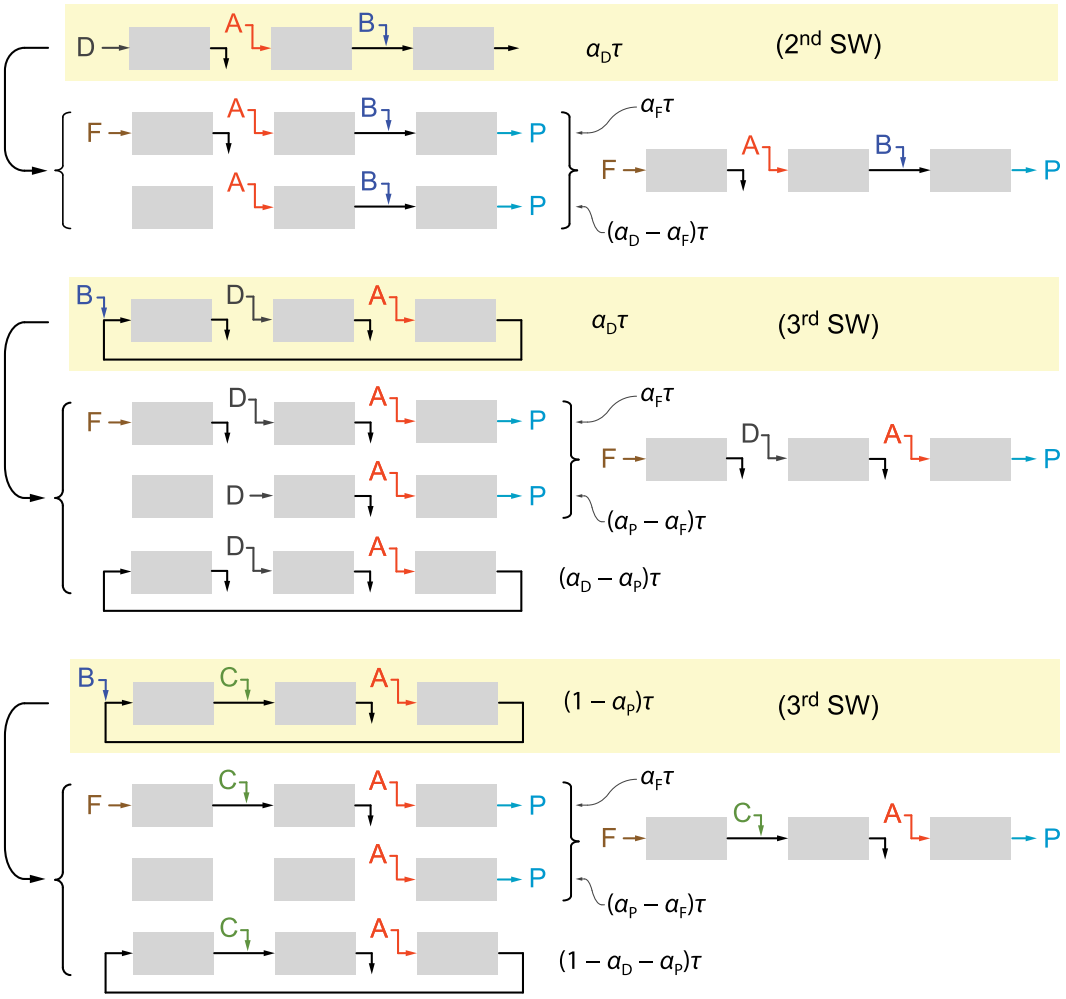

Fig. 2. Examples of steps where the feed is injected and the product collected at opposite ends of the column train; this sets the longest path between the feed inlet and product outlet. Each diagram enclosed in an yellow box is the configuration of the solvent lines (taken from Fig. 1) from which the immediately following feed/production diagram is derived. The subdivision of the steps is governed by parameters $\alpha_P \in (0, \alpha_D)$ and $\alpha_F \in (0, \alpha_P)$, except for the bottom case where $\alpha_P \in (0, 1 - \alpha_D)$. For modeling purposes, consecutive steps where the flow through one or more columns is halted can be merged into a single step; in this case, Q_F is replaced by w_F and α_F removed from the formulation.

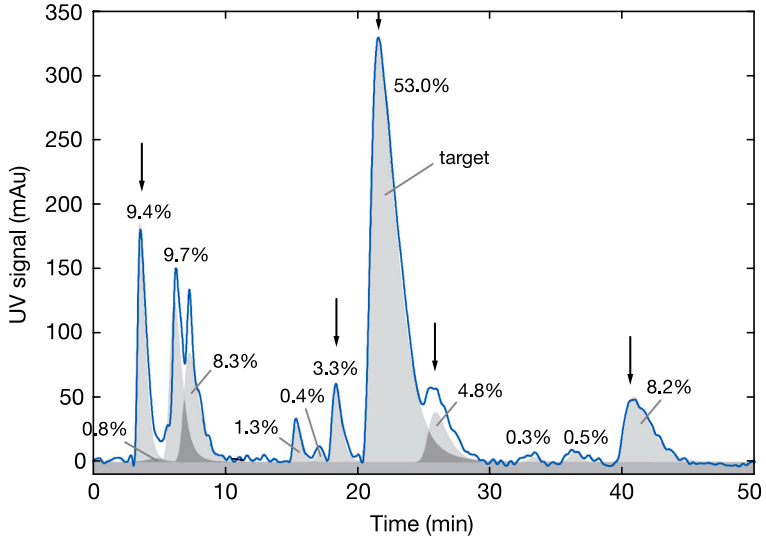

Fig. 3. Peak deconvolution of an analytical chromatogram of the crude peptide mixture. Column: Kromasil C18, 5 μm, 100 Å, 0.46 cm × 15 cm; solvent: water/ethanol/TFA (75/25/0.1, % (v/v)); flow rate: 0.5 ml/min; concentration: 1 g/l; injected volume: 250 μl; detector: UV 220 nm.

mixture, it is convenient to minimize the number of solutes taken into consideration in the design procedure to make it numerically tractable. Five key components were initially selected: weakest adsorbed (earliest eluting) impurity ($i = 1$), target product ($i = 3$) and its two closest impurities ($i = 2$ and $i = 4$), and strongest adsorbed (latest eluting) impurity ($i = 5$). The key components are identified by arrows pointing to their elution peaks in the analytical chromatogram of Fig. 3. This is the minimum set of solutes to be considered in the general case of linear adsorption where the Henry constants are monotonic functions of c_0 but their ordering does change with c_0. Later on it will be shown that to design the GSSR cycle it is enough to consider only three solutes (at least under linear adsorption conditions).

The total porosity of the chromatographic column is $\epsilon = \epsilon_b + (1 - \epsilon_b)\epsilon_p$, where ϵ_b is the interparticle void fraction and ϵ_p the intraparticle porosity. The total amount of solute i retained in the chromatographic column under equilibrium conditions per unit volume of empty column is $q_i = (\epsilon + H_i)c_i$, where c_i is the concentration of solute i in the liquid phase and H_i the Henry constant based on the same reference volume. Alternatively, q_i can be expressed as $q_i = [\epsilon + (1 - \epsilon_b)H_i']c_i$, where $H_i' = H_i/(1-\epsilon_b)$ is the Henry constant defined per unit volume of resin particle. This is just a matter of choice. When the extra column dead volume, V_e, is non-negligible, its contribution must be added to q_i; in this case, the simplest approach is to write the dependence of q_i on c_i as $q_i = (\epsilon + V_e/V_c + H_i)c_i$, where V_c is the geometrical column volume.

The Henry constants were fitted to the experimental data using the power-law correlation $H_i = H_i^0/c_0^{n_i}$, where the subscript i runs over the set of components ($i = 0$ represents EtOH, the solvent modifier), n_i is the power-law coefficient, c_0 the EtOH concentration (expressed as volumetric fraction), and H_i^0 the value of H_i when $c_0 = 1$. These values are listed in Table 1. It is worth noting that the values of H_0^0 and n_0 are zero, since it is assumed that EtOH does not adsorb.

Fig. 4 shows the effective selectivity of the resin for retaining each key impurity over the product as a function of the volumetric fraction of EtOH (c_0) in the mobile phase. The effective selectivity of the resin for key impurity i is defined as

$$\alpha_{i,3} = \frac{\epsilon + H_i}{\epsilon + H_3}, \tag{1}$$

where the index $i = 3$ identifies the product. This definition takes into account the retention in the liquid phase (interparticle void volume and intraparticle pore volume) and adsorbed phase but, for simplicity, does not include the effect of extra column dead volumes. These can be approximately account for by adding V_e/V_c to ϵ in the definition of $\alpha_{i,3}$. Fig. 4 shows that the resin is more selective (i.e., the difference in retention times is larger) at low EtOH concentrations because the Henry constants are monotonic decreasing functions of c_0; if c_0 is increased sufficiently, $\alpha_{i,3} \to 1$ and the resin loses almost all of its selectivity. Moreover, since the $\alpha_{i,3}$ curves do not cross, there is no selectivity reversal with a change in c_0. In short, low c_0 values ease up the separation of the mixture; high EtOH contents facilitate column cleanup and reduce the cycle time.

4. Problem formulation

The standard equilibrium-dispersive model (Ruthven, 1984) is used to predict the dynamics of the concentration profiles inside each column:

$$\left(\epsilon + \frac{V_e}{V_c}\right)\frac{\partial c_i}{\partial \theta} + \frac{H_i^0}{c_0^{n_i}}\left(\frac{\partial c_i}{\partial \theta} - \frac{n_i c_i}{c_0}\frac{\partial c_0}{\partial \theta}\right) = \frac{\tau Q}{V_c}\left(\frac{h_i}{2}\frac{\partial^2 c_i}{\partial x^2} - \frac{\partial c_i}{\partial x}\right), \tag{2}$$

where $x = z/L_c$ is a dimensionless axial coordinate scaled by the column length L_c, $\theta = t/\tau$ a dimensionless time coordinate scaled by the duration τ of each step of the cycle, Q the volumetric flow rate of mobile phase, and h the dimensionless plate height. The second term in the left-hand side of Eq. (2) is the expansion of $\partial(H_i c_i)/\partial\theta$. Also, note that for $i = 0$ (volumetric fraction of EtOH in the mobile phase), $H_0 = 0$ and $n_0 = 0$, so the left-hand side of Eq. (2) is simply $(\epsilon + V_e/V_c)(\partial c_0/\partial\theta)$.

Although the above equation includes only the component index i, c_i is also indexed over the set of columns and set of steps. To be more specific, the concentration profiles are multidimensional distributed variables $c_{ijk}(x,\theta)$, where $0 \le x \le 1$ is the dimensionless axial domain for column j, $0 \le \theta \le 1$ is the dimensionless time domain for step k ($d\theta = dt/\tau_k$), i runs over the set of components, j over the set of columns, and k over the set of steps of the cycle. The flow rate Q is effectively distributed over the set of columns and the set of steps of the cycle, i.e., Q_{jk} is the flow rate through column j during step k of the cycle. However, for simplicity's sake we shall stick to the simplified notation whenever possible.

The dimensional time, t, along step k of the cycle is related to θ as follows:

$$t = \tau_k\theta + \sum_{m=1}^{k-1}\tau_m, \quad dt = \tau_k d\theta. \tag{3}$$

The cycle time is simply $t_{cyc} = \sum\tau_k = N_c\tau$, where a subscripted τ, say τ_k, is the duration of a specific step in the cycle, whereas the non-subscripted τ represents the length of the switch interval.

The dimensionless plate height, h_i, governing the band broadening of the ith component, can be expressed as (Guiochon et al., 2006)

$$\frac{h_i}{2} \equiv \frac{1}{\mathrm{Pe}} = \frac{1}{\mathrm{Pe}_0} + \alpha_i\frac{Q}{V_c} + h_m\frac{V_c}{Q}, \tag{4}$$

$$\frac{1}{\mathrm{Pe}_0} = \frac{\gamma d_p}{L_c}, \quad h_m = \frac{\epsilon_b D_m}{\xi L_c^2}, \quad \alpha_i = \frac{\epsilon - \epsilon_b + H_i}{k(\epsilon + H_i)^2}. \tag{5}$$

The term $1/\mathrm{Pe}_0$ is the contribution of hydrodynamic dispersion ($\gamma \sim O(1)$ is a constant), $h_m V_c/Q$ the contribution of molecular diffusion (D_m is the molecular diffusion coefficient and ξ the tortuosity factor), and $\alpha_i Q/V_c$ the contribution of mass transfer and intraparticle diffusion (k is the LDF coefficient for mass transfer). The values of these parameters are listed in Table 1.

Eq. (2) can be rewritten as

$$\left(\epsilon + \frac{V_e}{V_c}\right)\frac{\partial c_i}{\partial\theta} + \frac{\partial q_i}{\partial\theta} = w\left[\left(\frac{1}{\mathrm{Pe}_0} + \frac{\alpha_i w}{\tau}\right)\frac{\partial^2 c_i}{\partial x^2} - \frac{\partial c_i}{\partial x}\right] + \tau h_m\frac{\partial^2 c_i}{\partial x^2}, \tag{6}$$

where $w \equiv \tau Q/V_c$ is the volume of fluid eluted per unit volume of empty column over the interval τ and the three contributions to the dimensionless plate height are made explicit.

The differential material balance is subject to the usual boundary conditions

$$Q\left(c_i - \frac{h_i}{2}\frac{\partial c_i}{\partial x}\right) = (Qc_i)_{in}, \tag{7}$$

$$\frac{\partial c_i}{\partial x} = 0, \tag{8}$$

where $(Qc_i)_{in}$ is the inlet mass (or molar) flowrate of component i. The upstream boundary condition can also be rewritten in terms of w:

$$w\left[c_i - \left(\frac{1}{\mathrm{Pe}_0} + \frac{\alpha_i w}{\tau}\right)\frac{\partial c_i}{\partial x}\right] - \tau h_m\frac{\partial c_i}{\partial x} = (wc_i)^{in}. \tag{9}$$

This upstream boundary condition is the main reason why the molecular diffusion term ($\tau h_m \partial c_i/\partial x$) is not neglected. If the flow through the column is halted ($Q = 0$), only when $h_m \neq 0$ does the above boundary condition reduce to the correct expression

$$\left(\frac{\partial c_i}{\partial x}\right)_{x=0} = 0. \tag{10}$$

On the contrary, if $h_m = 0$ and $Q = 0$, the boundary condition becomes indeterminate ($0 = 0$), which can cause numerical problems for some computational solvers.

Under cyclic steady state (CSS) conditions the axial concentration profiles at the beginning and end of a cycle are equal. This condition is imposed directly in the optimization problem as a constraint:

$$c_{i,j,1}(x, \theta = 0) = c_{i,j,M}(x, \theta = 1) \quad \forall i, j, x, \tag{11}$$

where M is the number of steps per cycle.

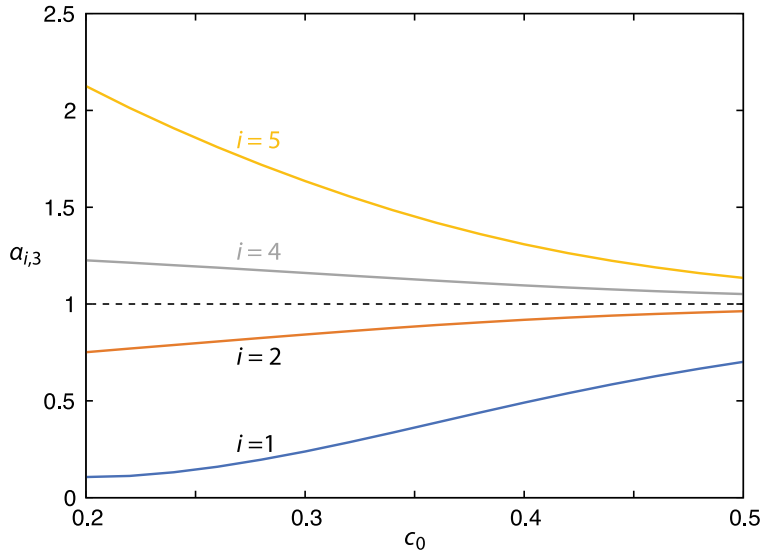

Fig. 4. Effective selectivity of the resin for retaining each key impurity i over the product, $\alpha_{i,3} = (\epsilon + H_i)/(\epsilon + H_3)$ where H_i is the Henry constant of solute i (the product is $i = 3$), as a function of the volumetric fraction of EtOH in the mobile phase (c_0).

Table 1
Process parameters. They are all dimensionless, except D_m which is given in cm^2/min and k in min.

i	1	2	3	4	5
H_i	8×10^{-7}	0.016	0.016	0.018	0.017
n_i	8.36	3.83	4.02	4.08	4.47
ϵ	0.61	ϵ_b	0.4	ξ	3.0
D_m	1.5×10^{-5}	k	0.0035	γ	0.7

The amount of component i collected per cycle and unit volume of empty column is

$$y_i = \sum_{k\in\mathcal{P}} \frac{\tau_k Q_{3,k}}{V_c} \int_0^1 c^{\text{out}}_{i,3,k}\, d\theta = \sum_{k\in\mathcal{P}} w_{3,k} \int_0^1 c^{\text{out}}_{i,3,k}\, d\theta, \tag{12}$$

where $c^{\text{out}}_{ijk}(\theta)$ is the temporal concentration profile of component i at the outlet of column j during step k of the cycle, $Q_{3,k}$ the volumetric flowrate in column 3 during step k, $w_{3,k} \equiv Q_{3,k}\tau_k/V_c$ the corresponding volume of mobile phase eluted per unit volume of empty column during step k, and $\mathcal{P}$ the set of steps over which the product is collected from the process via column 3. The fraction with the purified product will almost always be collected during a single step of the cycle, so the cardinality of $\mathcal{P}$ will normally be unitary.

The product purity, P, is simply

$$P = \frac{y_p}{\sum_{i\in S} y_i}, \tag{13}$$

where p is the target component and S the set of solutes (excluding the solvent modifier). The product recovery, R, is given by

$$R = \frac{y_p}{c_p^F w_F}, \tag{14}$$

where c_p^F is the concentration of the target component in the feed stream and w_F the number of empty column volumes of feed injected per cycle into the process via column 1. One is usually interested in operating the process as close as possible to the maximum throughput, which in turn is proportional to the average feed flowrate per cycle:

$$\overline{Q}_F = \frac{w_F}{\sum_k \tau_k}. \tag{15}$$

The goal of the optimization procedure is to optimally design the process so that $\overline{Q}_F$ is maximized while satisfying the purity and recovery constraints:

$$P \geq P_{\min}, \quad \text{and} \quad R \geq R_{\min}. \tag{16}$$

The first thing to notice in preparative chromatography is that it is ultimately governed by the products $w_{jk} \equiv \tau_k Q_{jk}/V_c$, that is, the number of empty column volumes of mobile phase eluted through column j in step k, and not by the individual values of τ_k and Q_{jk}. This is apparent from the equilibrium-dispersive model and the purity and recovery constraints. Moreover, if the stationary phase is reasonably efficient, the operating flow rates will ultimately be constrained by the pressure drop. The only exception in this line of reasoning is the objective function, aka $\max \overline{Q}_F$, which cannot be expressed solely as a function of the w_{jk} unless the cycle time is fixed.

To appreciate the advantages of formulating the problem in terms of w, consider, for example, the following two steps of the cycle:

$$\begin{array}{lllllll} (\tau_5) & \text{F} \rightarrow & \boxed{1} & \text{D} \rightarrow & \boxed{2} & \text{A} \rightarrow & \boxed{3} \rightarrow \text{P} \\ (\tau_6) & & \boxed{1} & \text{D} \rightarrow & \boxed{2} & \text{A} \rightarrow & \boxed{3} \rightarrow \text{P} \end{array} . \tag{17}$$

This sequence occurs frequently because the volume of feed injected per cycle is usually less than the volume of the collected fraction with purified product. In addition to the two step lengths, τ_5 and τ_6, the operating variables for these two steps are the feed flow rate, Q_F, and the two solvent flow rates, Q_A and Q_D. However, to a very good approximation these two steps can be merged into a single one:

$$(\tau_5') \quad w_F \rightarrow \boxed{1} \quad w_D \rightarrow \boxed{2} \quad w_A \rightarrow \boxed{3} \rightarrow w_D \ , \tag{18}$$

where $\tau_5' = \tau_5 + \tau_6$ and $V_c w_j = (\tau_5 + \tau_6) Q_j$. This type of formulation easily handles situations where either Q_B or Q_C is zero but the other is not, or both are null.

Given that $w_{jk} \propto Q_{jk}\tau_k$, the choice of the flow rates and τ as decision variables gives rise to an ill-conditioned optimization problem, unless a maximum operating flow rate constraint is included (e.g., via a pressure drop constraint). It is better to fix τ and keep the flow rates or w's as decision variables or else to fix one flow rate at a reference value and keep τ as decision variable.

The positioning in the cycle and duration of both feed injection and product collection are also decision variables, but, as mentioned above, they are synchronized for optimal performance (Fig. 2). The duration of product withdrawal is defined as a fraction $0 \leq \alpha_P \leq 1$ of the sw, i.e., a time interval of length $\alpha_P \tau$. As explained above, it is better to choose w_F as decision variable instead of Q_F, as this reduces the number of cycle steps that have to be considered. Otherwise, it is also necessary to take into account that the feed is injected during a fraction α_F of the switch interval (time interval with duration $\alpha_F \tau$).

Each switch interval is divided into two sub-steps, the first with duration $\alpha_D\tau$ and the other with length $(1-\alpha_D)\tau$. Obviously, α_D is a decision variable. The step durations are simply

$$\tau_k = \alpha_k\tau, \quad \alpha_k = \begin{cases} \alpha_D & \text{if} \quad k = 1,3,5 \\ 1-\alpha_D & \text{if} \quad k = 2,4,6 \end{cases} . \tag{19}$$

The remaining decision variables are the initial and final concentrations of EtOH in the linear gradient of solvent A. The time-periodic concentration profile of EtOH in solvent A, $c_A(\theta)$, can be conveniently defined in terms of α_D and θ, the latter being the dimensionless time coordinate of each step:

$$c_A(\theta) = c'_A + (c''_A - c'_A) \times \begin{cases} \alpha_D\theta & \text{if} \quad k = 1,3,5 \\ \alpha_D + (1-\alpha_D)\theta & \text{if} \quad k = 2,4,6 \end{cases} . \tag{20}$$

Henceforth, we do not use an index to indicate the solute concentration in a given solvent Note that if the feed injection and product collection occur during the third switch interval, as is advisable, they do not interfere with the normal operation of solvent A.

Let $w_A \equiv Q_A\tau/V_c$, $w_B \equiv Q_B\tau/V_c$, $w_C \equiv Q_C(1-\alpha_D)\tau/V_c$, and $w_D \equiv \alpha_D Q_D/V_c$ be the number of empty column volumes of each solvent injected per switch interval if the process were undisturbed by feed injection and product withdrawal (cf. Fig. 1). Or in other words, the number of empty column volumes of solvent injected in every switch interval expect the one where feed and production take place. Let $w_F \equiv Q_F\alpha_F\tau$ be the number of empty column volumes of feed injected per cycle. Then, all w_{jk}'s can be defined in terms of these variables. For example, according to the schematic of Fig. 1 the number of empty column volumes of fluid injected into the columns during the first step of the cycle are (column 1) $w_{1,1} = \alpha_D w_A$, (column 2) $w_{2,1} = w_{1,1} + \alpha_D w_B$, and (column 3) $w_{3,1} = w_D$. The number of empty column volumes of fluid injected into the columns during the second step of the cycle are (column 1) $w_{1,2} = (1-\alpha_D)w_A$; (column 2) $w_{2,2} = w_{1,1} + (1-\alpha_D)w_B$; and (column 3) $w_{3,1} = w_{3,2} + w_C$.

If one adopts a formulation that employs w_F instead of Q_F, the basic building blocks of the cycle are the following: A→, D→, F→, →, $\xrightarrow{B\downarrow}$, and $\xrightarrow{C\downarrow}$. The first three blocks are direct injection of the column with feed or solvent, the fourth is feeding the column with the upstream effluent, and the fifth and sixth are admixing the column with the upstream effluent and solvent. The cycle can be defined using a symbolic matrix S, where each element indicates the corresponding building block: A, D, F, O, B, and C. For example,

$$S = \begin{array}{c} (k,j) \\ 1 \\ 2 \\ 3 \\ 4 \\ 5 \\ 6 \end{array} \begin{array}{c} \begin{array}{ccc} 1 & 2 & 3 \end{array} \\ \left[\begin{array}{ccc} A & B & D \\ A & B & C \\ D & A & B \\ C & A & B \\ F & D & A \\ B & C & A \end{array}\right] \end{array} \quad \begin{array}{l} A\rightarrow\blacksquare\rightarrow(+B)\rightarrow\blacksquare\rightarrow \quad D\rightarrow\blacksquare\rightarrow \\ A\rightarrow\blacksquare\rightarrow(+B)\rightarrow\blacksquare\rightarrow(+C)\rightarrow\blacksquare\rightarrow \\ D\rightarrow\blacksquare\rightarrow \quad A\rightarrow\blacksquare\rightarrow(+B)\rightarrow\blacksquare\rightarrow \\ (+C)\sqsubset\blacksquare\rightarrow \quad A\rightarrow\blacksquare\rightarrow(+B)\rightarrow\blacksquare\rightarrow\!\!\lrcorner \\ F\rightarrow\blacksquare\rightarrow \quad D\rightarrow\blacksquare\rightarrow \quad A\rightarrow\blacksquare\rightarrow P \\ (+B)\sqsubset\blacksquare\rightarrow(+C)\rightarrow\blacksquare\rightarrow \quad A\rightarrow\blacksquare\rightarrow\!\!\lrcorner \end{array} , \tag{21}$$

where k runs over the set of steps, j over the set of columns, and $\sqsubset\!\rightarrow$ $\rightarrow\!\!\lrcorner$ means that the effluent at the downstream end of the system is recirculated back to the upstream end. This is one example of cycle where both feed injection and product withdrawal start at the beginning of the third switch interval and $\alpha_P = \alpha_D$. From the elements of S the volumes and amounts of each component injected per column and per step are easily obtained:

$$w_{jk} = \begin{cases} \alpha_k w_A & (S_{kj} = A) \\ \alpha_k w_B + w_{j-1,k} & (S_{kj} = B) \\ w_C + w_{j-1,k} & (S_{kj} = C) \\ w_{j-1,k} & (S_{kj} = O) \\ w_D & (S_{kj} = D) \\ w_F & (S_{kj} = F) \end{cases} , \tag{22}$$

$$(wc_0)^{in}_{jk} = \begin{cases} (wc_0)_D & (S_{kj} = D) \\ (wc_0)_F & (S_{kj} = F) \\ \alpha_k(wc_0)_A & (S_{kj} = A) \\ \alpha_k(wc_0)_B + (wc_i)^{out}_{j-1,k} & (S_{kj} = B) \\ (wc_0)_C + (wc_i)^{out}_{j-1,k} & (S_{kj} = C) \\ (wc_i)^{out}_{j-1,k} & (S_{kj} = O) \end{cases} ,$$

$$(wc_{i\neq 0})^{in}_{jk} = \begin{cases} 0 & (S_{kj} = A, D) \\ (wc_i)^{out}_{j-1,k} & (S_{kj} = B, C, O) \\ (wc_i)^{F} & (S_{kj} = F) \end{cases} . \tag{23}$$

Here, $(wc)_A$, $(wc)_B$, ... are shorthands for $w_A c_A$, $w_B c_B$, ...; also note that $c_A \equiv c_A(\theta)$ is the time-periodic EtOH concentration in the linear solvent gradient, while c_B, c_C, ... are the constant EtOH concentrations in the isocratic solvents.

5. Solution procedure

The differential–algebraic nonlinear programming (DANLP) problem is solved directly for steady-periodic process operation, i.e., for cyclic steady state (CSS) conditions. To this end, a full discretization approach for steady-period dynamics is applied to the DANLP problem, which converts it into a large, sparse, algebraic nonlinear programming (NLP) problem (see §2 of Supporting Information).

The algebraic NLP problem obtained after discretization is formulated in AMPL (AMPL) and solved with the interior-point optimizer IPOPT (Wächter and Biegler, 2006), ver. 3.12.3 (COIN-OR, 2022) (see §3 of Supporting Information). This solution strategy has been previously employed with success by our group on a broad class of SMB problems (Araújo et al., 2006; Rodrigues et al., 2007b,a; Mota et al., 2007b). Our version of IPOPT has been compiled with OpenBLAS (OpenBLAS, 2022), an efficient implementation of BLAS (Basic Linear Algebra Subroutines) and LAPACK (Linear Algebra PACKage), tailored to our hardware. IPOPT also requires at least one linear solver for sparse symmetric indefinite matrices. The linear solver used in the present work is the Watson Sparse Matrix Package WSMP (Gupta, 2000), ver. 20.09.18 (Anon, 2021).

6. Results and discussion

Although a generic formulation should in principle include the solvent modifier and five key components (see Table 1), we start with the simpler quaternary mixture that includes the solvent modifier and only three solutes: the target product and its two nearest neighbors. This significantly reduces (by a third) the problem size compared to a formulation that also includes the weakest and strongest adsorbed impurities.

Starting from an initial estimate of the decision variables, we proceed as follows. First, the optimization problem is temporarily dropped, and for the initial estimate of the decision variables, the steady periodic EtOH concentration profile, $c_{0,j,k}(x,\theta)$, is determined, since it does not depend on the solute concentration profiles. This is a large, but sparse, system of linear equations involving 163080 unknowns and $O(10^6)$ nonzero coefficients, but far less than $O(10^{10})$ if the system were fully dense. The linear system is solved using IPOPT/WSMP as a linear programming problem with only equality constraints and no objective function. The high-performance WSMP parallel sparse linear solver working with 16 threads solves the problem in 18 s.

Then, the steady periodic solute concentration profiles, $c_{i\neq 0,j,k}(x,\theta)$, are computed. Again, this is a linear problem because the adsorption isotherm is a linear function of the solute concentration and the previously determined EtOH concentration profile is now kept fixed. The concentration profile of each solute can be calculated one at a time (this would be the fastest way) or all at the same time. We choose the latter option for simplicity. This linear problem involves 489240 unknowns if the formulation includes three solutes and the corresponding matrix

has $3 \times O(10^6)$ nonzeros. This problem is solved by IPOPT/WSMP in 70 s.

Now that the concentration profiles have been calculated for the initial estimate of the decision variables, the EtOH concentration profile is unfixed (it had been fixed to facilitate the calculation of the solute concentration profiles), the purity and recovery constraints and objective function are added to the problem, the decision variables are unfixed, and the optimization problem is solved. To get an idea of the size and complexity of the NLP problem, note that if all the potential decision variables are unfixed, the problem has 652329 variables, of which 615609 appear in nonlinear expressions, 652322 equality constraints, of which 417604 are nonlinear, and two hard inequality constraints (restrictions of the type $0 \le Q_A \le Q_{max}$, $0 \le \alpha_D \le 1$, etc., are not being taken into account here).

The initial estimate of the decision variables is the operating point previously determined by us (Silva et al., 2010): $\tau = 3.5$ min, $\alpha_D = 0.429$ $(1.5/\tau)$, $\alpha_F = 0.143$ $(0.5/\tau)$, $\alpha_P = 0.286$ $(1.0/\tau)$, $Q_A = 5.7$ ml/min, $Q_B = 1.0$ ml/min, $Q_C = 1.25$ ml/min, $Q_D = 5.0$ ml/min, $Q_F = 2.0$ ml/min, $c'_A = 0.324$, $c''_A = 0.354$; the EtOH concentrations in the isocratic solvents are fixed at $c_B = c_C = 0.25$ v/v, and $c_D = 0.5$ v/v. The process throughput for this operating point is $\overline{Q}_F = 0.095$ ml/min of processed feed.

Consider first the simpler problem of maximizing $\overline{Q}_F$ subject to $P_{min} = R_{min} = 0.98$ by manipulating the cycle times but keeping the flow rates and solvent compositions fixed at their initial values. This optimization problem takes ca. 13 min of CPU time to solve in our machine. The optimal values obtained for the decision variables are $\tau = 3.56$ min and $\alpha_F = \alpha_P = \alpha_D = 0.330$, corresponding to a maximized value $\overline{Q}_F = 0.220$ ml/min of processed feed. In this optimized configuration the fifth step in Fig. 1 is replaced in its entirety by the two sub-steps shown in Eq. (17); see also the middle sequence in Fig. 2 for comparison. This numerical experiment indicates that the original values of the process times are conservative and can be improved. Note, however, that this comparison may not be completely legitimate because Silva et al. (2010) most likely wanted to make sure that the experimental runs were performed in the linear range of the adsorption equilibrium.

However, the fact that the optimal solution gives $P = P_{min}$ but $R \sim 0.995 > R_{min}$ means that the formulation of the optimization problem is too restrictive, thus preventing the purity and recovery constraints from being satisfied by only an infinitesimal margin. The problem resides in that the values of all operating flow rates were fixed. To relax the problem, Q_F is replaced by w_F as decision variable (consequently, α_F is dropped from the problem) and the formulation changed to one in which the two sub-steps in Eq. (17) are merged into the single one given in Eq. (18). The revised NLP problem is solved using as decision variables τ, α_P, α_D, and w_F. This optimization took ca. 30 min of CPU time. The optimal values obtained for the decision variables are $\tau = 3.50$ min, $\alpha_P = \alpha_D = 0.331$, $w_F = 1.448$ ($Q_F = 9.83$ ml/min), and $P = R = 0.98$; the computed productivity is $\overline{Q}_F = 1.08$ ml/min of processed feed. This is a significant result: it is possible to process $1.08/0.095 \sim 11$ times more feed per cycle than originally foreseen.

Next we check whether the process can be further improved by optimizing the EtOH gradient in solvent A. Given that the previous optimization gave $Q_F = 9.83$ ml/min, the feed flow rate is also constrained not to exceed 10 ml/min. To optimize the modifier gradient, variables c'_A and c''_A are added to the set of unfixed decision variables and the process is optimized subject to the additional constraints $0.25 \le c'_A \le 0.5$ and $0.25 \le c''_A \le 0.5$; here, 0.25 v/v is the modifier concentration in the feed and in solvents B and C, while 0.5 v/v is the concentration in solvent D. The optimal values of the decision variables given by the solution of this NLP problem are $\tau = 3.53$ min, $\alpha_P = \alpha_D = 0.330$, $w_F = 1.483$ ($Q_F = 10.0$ ml/min), $c'_A = 0.293$ v/v, and $c''_A = 0.428$ v/v. The purity and recovery constraints are satisfied at their lower limits ($P = R = 0.98$), and the computed productivity is $\overline{Q}_F = 1.10$ ml/min of processed feed.

Finally, we explore the possibility of reducing the solvent consumption without penalizing the productivity, or doing so minimally. Since solvents B and C are isocratic with modifier concentrations $c_B = c_C = 0.25$ v/v, in principle it is possible to substitute their effect, if only partially, by steeping the modifier gradient of solvent A. We thus fix $Q_B = Q_C = 0$ ml/min and let the algorithm find the optimal values of c'_A and c''_A. Since minimizing the consumption of solvent D is also a desirable goal, we consider the following objective function:

$$\min_{\mathcal{V}} (\overline{Q}_F - \mu w_D), \quad \mathcal{V} = \{\tau, \alpha_P, \alpha_D, w_F, w_D, c'_A, c''_A\}, \tag{24}$$

where $\mathcal{V}$ is the set of decision variables and $\mu > 0$ a small positive parameter that penalizes the use of solvent D.

The optimal results for this formulation ($\mu = 10^{-3}$) are $Q_A = 5.7$ ml/min, $\tau = 4.20$ min, $\alpha_P = \alpha_D = 0.281$, $Q_B = Q_C = 0$ ml/min, $w_D = 0.0$, $w_F = 1.949$ ($Q_F = 12.98$ ml/min), $c'_A = 0.25$ and $c''_A = 0.424$, for which $P = 0.98$, $R = 0.98$, and $\overline{Q}_F = 1.21$ ml/min. Here, the constraint $Q_F \le 10$ ml/min was relaxed, as it was observed that the optimal value of w_F gives a Q_F of just over 10 ml/min. Overall, this operating point is very appealing, as it eliminates the use of solvents B, C, and D without compromising the process throughput.

It is important to keep in mind that the IPOPT's algorithm only tries to find a local minimizer of the NLP problem; if the problem is nonconvex, as is the case under study here, many stationary points with different objective function values might exist, and it depends on the starting point and algorithmic choices which particular one the method converges to. We did not evaluate the sensitivity of the optimal solution with respect to the initial starting point, nor was it thought necessary to use a multistart method to seek a globally optimal solution. The latter strategy would entail automatically starting IPOPT from randomly selected starting points, eventually reaching different locally optimal solutions, and then selecting the best of these as the proposed globally optimal solution.

After each of the optimizations reported above, the weakest and strongest adsorbing impurities were added to the set of solutes and the steady periodic solution was recalculated for the previously determined optimal operating point. The values of P and R never changed. This is a significant result: although the weakest and strongest adsorbing impurities were not considered in the optimization procedure, they are completely rejected by the process as waste and therefore do not affect the product purity.

To help further analyze the metrics of the operating points, two Key Performance Indicators (KPIs) are used: the concentration ratio, R_C, and the solvent consumption ratio, R_{SC}. The former compares the concentration of the target component in the product fraction with that in the feed stream:

$$R_C = \frac{y_p}{c_p^F \sum_{k \in \mathcal{P}} w_{3,k}}, \tag{25}$$

where y_p is the amount of target component collected per cycle and per column volume, as given by Eq. (12), w_{jk} the number of empty column volumes of fluid eluted through column j during step k, and $\mathcal{P}$ the set of steps over which the product is collected from the process via column 3. Obviously, the larger the value of R_C, the better. Alternatively, the dilution ratio, $R_D = 1/R_C$, which is just the inverse of R_C, can be used. Obviously, in this case the smaller the value of R_D, the better. The solvent consumption ratio, R_{SC}, is given by the sum of the volumes of solvents A, B, C, and D used per cycle divided by the volume of feed injected per cycle.

Table 2 summarizes the metrics of the optimal operating points resulting from the various optimizations. The last three operating points have R_C values larger than 1 and R_{SC} values smaller than 10. Note that $R_C > 1$ means that the target component is more concentrated in the collected product fraction than in the feed stream. Also, because the

Table 2
Metrics of the optimal operating points resulting from the various process optimizations for $P \geq 0.98$ and $R \geq 0.98$. The first row is the operating point reported by Silva et al. (2010). The flowrates are in ml/min; τ in min; c'_A, c''_A in v/v; w_F and w_D in ml of fluid per ml of column; all other measures are dimensionless.

τ	α_D	α_F	α_P	Q_A	Q_B	Q_C	w_F	w_D	c'_A	c''_A	$\overline{Q}_F$	R_C	R_{SC}
3.50	.429	.143	.286	5.7	1.0	1.25	.127	.955	.324	.354	.095	.110	59.9
3.56	.330		.330	5.7	1.0	1.25	.299	.749	.324	.354	.220	.349	41.2
3.50	.331		.331	5.7	1.0	1.25	1.45	.736	.324	.354	1.08	1.69	8.38
3.53	.330		.330	5.7	1.0	1.25	1.48	.741	.293	.428	1.10	1.72	8.25
4.20	.281		.281	5.7	0.0	0.00	1.95	.000	.250	.424	1.21	2.23	4.70

last operating point works without solvents B, C, and D, its R_{SC} value is much smaller than those of the other operating points.

Fig. 5 shows the full GSSR cycle for the operating point given in the last row of Table 2, along with snapshots of the simulated axial concentration profiles in the three columns taken at selected instants of the cycle when switching between some of the steps. The concentration profiles have been scaled by the corresponding concentrations in the feed for better visualization; this makes it possible to zoom in on the impurity profiles, which would otherwise be difficult to discern at some stages of the cycle. The horizontal line with large dashes represents the dimensionless feed concentration.

Fresh feed is injected at the upstream end of the open-loop train of columns at the beginning of the third switch interval, while at the same time the target component is obtained in purified form at the downstream end of the system. In this way, each feed pulse injected per cycle is forced to travel the entire length of the system to maximize the separation between neighboring peaks. The cut containing the leading edge of the product mixed with the nearest slightly less adsorbed impurity is recycled to the upstream end of the system; only then does the product collection begin. Product withdrawal continues until breakthrough of the nearest slightly more adsorbed impurity. Then, the cut containing this impurity mixed with the trailing edge of the target component is recycled to the upstream end of the system. This cut is injected into the upstream end of the system right after the injection of feed.

To better observe the internal recycling of the mixed fractions from the downstream end to the upstream end of the system, Fig. 6 shows similar graphical information as Fig. 5, but for an optimized cycle where the concentration of the target component in the feed, c_p^F, was lowered from 0.53 to 0.23 and the minimum acceptable purity and recovery values increased to 0.99. Thus, whereas in the previous case the target product is 53% of the feed, it now represents only 33% ($100\times 0.23/(0.23+1-0.53)$). The GSSR metrics for this case are $\tau = 5.80$ min, $\alpha_D = \alpha_F = \alpha_P = 0.226$, $Q_A = Q_B = Q_C = 0$ ml/min, $w_F = 1.243$, $w_D = 0$, $c'_A = 0.25$ v/v $c''_A = 0.309$ v/v, $\overline{Q}_F = 0.561$ ml/min, $R_C = 1.28$, $R_{SC} = 10.2$. Obviously, increasing the relative content of the impurities—especially the two closest to the key component—and upping the purity and recovery specifications worsens the process metrics: $\overline{Q}_F$ decreases from 1.21 to 0.561 ml/min and R_{SC} increases from 4.70 to 10.2 when c_p^F is reduced from 0.53 to 0.23 without changing the impurity content in the feed. The lower amount of feed processed per cycle and higher solvent consumption increase the dilution rate of the solutes in the mobile phase, as can be seen by the different scales on the left y-axis in Figs. 5 and 6.

Fig. 7 summarizes the influence of c_p^F on τ, α_D, $\overline{Q}_F$, and c''_A for $P_{min} = R_{min} = 0.98$ and fixed concentrations of the impurities in the feed. Note that c'_A is always equal to 0.25 v/v, so increasing the value of c''_A is equivalent to steeping the modifier gradient of solvent A. Fig. 7 shows that all parameters increase with increasing c_p^F except τ which follows the opposite trend.

Fig. 8 shows how the purity and recovery change as some operating parameters are moved away from their optimal values. The parametric analysis includes τ, w_F, c''_A, and $\alpha_F = \alpha_P = \alpha_D$. For example, $\delta\tau = +2\%$ means that τ is 2% longer than its optimum value, while $\delta w_F = -2\%$ means that w_F is 2% smaller than its optimum value. Overall, the recovery is more affected than purity by a deviation of any of these parameters from its optimal value. Either a positive or negative deviation of τ or c''_A from the optimal value causes a decrease in purity and recovery, but R is much more penalized than P. On the other hand, both P and R are monotonic functions of δw_F and $\delta\alpha_D$ for small changes of w_F or α_D. The purity is slightly penalized by a positive deviation of w_F or α_D and slightly improved if the parameter deviates negatively from its optimum value. The recovery, however, improves with increasing $\delta\alpha_D$ but worsens with increasing δw_F.

In practice a GSSR unit uses a distributed valve design based on two-way or multi-way valves to implement the port switching. Since, for all intents and purposes, the valve switching is instantaneous, the uncertainty in the experimental cycle times (τ, α_D, α_F, and α_P) should be very small. The uncertainty in w_F is mostly dependent on the experimental variability of the feed pump. Of all the variables considered, c''_A seems to be by far the one subject to the largest experimental uncertainty.

Suppose the modifier gradient is generated from two solvent solutions: one with a modifier concentration of 0.25 v/v and the other 0.5 v/v. Recall that these are the boundary values considered earlier for all solvents. Since the optimal value of the initial gradient is $c'_A = 0.25$ v/v, as a good approximation this concentration is generated experimentally without any uncertainty because it does not required admixing of the two solvent solutions. On the other hand, it is assumed that the experimental realization of c''_A is subject to an error, or uncertainty, that is bounded by a maximum relative deviation $\hat{\sigma}_A$, from its nominal value $\bar{c}''_A$:

$$c''_A = \bar{c}''_A + \sigma_A, \quad -\hat{\sigma}_A \leq \sigma_A \leq \hat{\sigma}_A. \tag{26}$$

Let $c = h^{CSS}(\mathcal{V}, \mathcal{P}, \sigma_A)$ be the solution of the steady periodic concentration profiles for given values of the set of decision variables $\mathcal{V} = \{\tau, \alpha_D, w_F, c'_A, \bar{c}''_A\}$, set of parameters $\mathcal{P}$ (geometrical dimensions of the column, porosity, adsorption parameters, etc.), and deviation σ_A. In the absence of uncertainty in the experimental value of c''_A ($\hat{\sigma}_A = 0$, $c''_A = \bar{c}''_A$), the mathematical programming problem for optimal GSSR design can be formulated as follows:

$$\max_{\mathcal{V}} \ \overline{Q}_F \tag{27}$$

$$\text{s.t. } c = h^{CSS}(\mathcal{V}, \mathcal{P}, 0), \tag{28}$$

$$P(c, \mathcal{V}, \mathcal{P}) \geq P_{min}, \tag{29}$$

$$R(c, \mathcal{V}, \mathcal{P}) \geq R_{min}. \tag{30}$$

When c''_A is subject to uncertainty, the best operating point must be chosen only among candidate solutions that are robust feasible, that is, that remain feasible whatever the perturbation of c''_A given by Eq. (26). If the solution is known to lie at one boundary the uncertainty region, the nominal problem given by Eqs. (27)–(30) can be replaced by a worst-case problem containing the vertices of the uncertainty region that most adversely affect the quality constraints. In other words, the shape of the curves in the upper-right plot of Fig. 8 allows us to conclude that the worst case scenarios are those where $c''_A = (1-\hat{\sigma}_A)\bar{c}''_A$ and $c''_A = (1+\hat{\sigma}_A)\bar{c}''_A$. If the purity and recovery constraints are satisfied for these two cases, they will also necessarily be satisfied for any intermediate case.

Thus, the optimal operating conditions when c''_A is subject to the uncertainty given by Eq. (26) can be obtained by solving the following robust NLP problem (Mota et al., 2007a; Nestola et al., 2015):

$$\max_{\mathcal{V}} \ \overline{Q}_F \tag{31}$$

$$\text{s.t. } c^- = h^{CSS}(\mathcal{V}, \mathcal{P}, 1-\hat{\sigma}_A), \tag{32}$$

$$c^+ = h^{CSS}(\mathcal{V}, \mathcal{P}, 1+\hat{\sigma}_A), \tag{33}$$

$$P(c^-, \mathcal{V}, \mathcal{P}) \geq P_{min}, \quad P(c^+, \mathcal{V}, \mathcal{P}) \geq P_{min}, \tag{34}$$

$$R(c^-, \mathcal{V}, \mathcal{P}) \geq R_{min}, \quad R(c^+, \mathcal{V}, \mathcal{P}) \geq R_{min}, \tag{35}$$

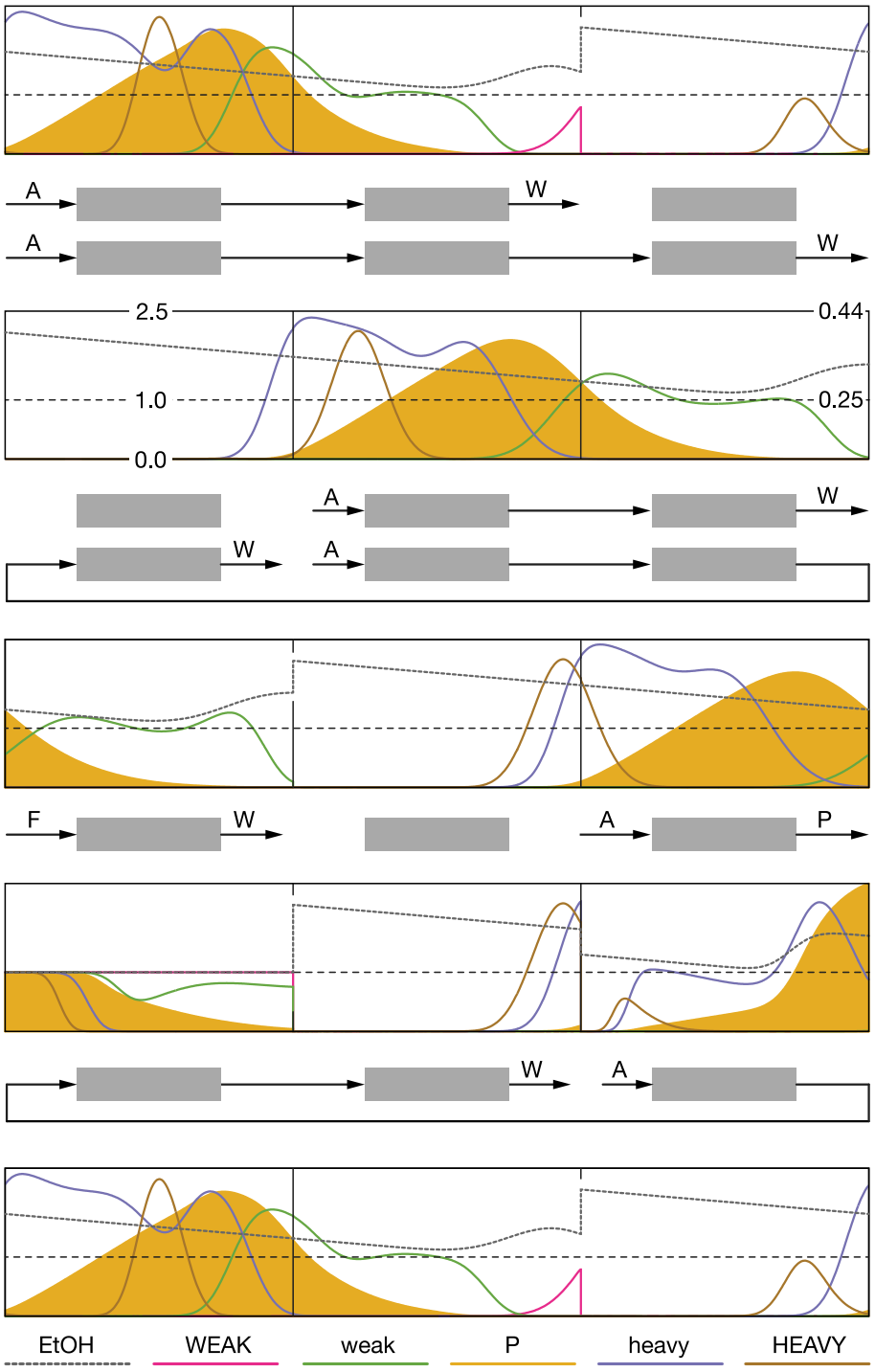

Fig. 5. Axial concentration profiles (c_i/c_i^F) in liquid phase under cyclic steady-state conditions for the last optimization result given in Table 2. Each solute concentration (c_i) is scaled by its value in the feed (c_i^F) and is read on the left y-axis. The dashed horizontal line represents the dimensionless feed concentration. The EtOH volume fraction is read on the right y-axis. The time instants at which the profiles are reported are from top to bottom: initial of the cycle, after one and two switch intervals, after the feed step, at the end of the cycle.

In other words, the robust NLP problem consists of two simultaneous instances of the nominal NLP problem linked by the same values of the decision variables $\mathcal{V}$ and parameters $\mathcal{P}$, but with $c''_A = (1-\hat{\sigma}_A)\overline{c}''_A$ in one instance and $c''_A = (1+\hat{\sigma}_A)\overline{c}''_A$ in the other.

This robust NLP is twice the size of the nominal NLP problem but still computationally tractable. The optimal values of the decision variables for $\sigma_A = 0.02$ (2%) are $\tau = 5.29$ min, $\alpha_F = \alpha_P = \alpha_D = 0.267$, $w_D = 0$, $w_F = 8.06$ ($Q_F = 5.70$ ml/min and $\overline{Q}_F = 0.507$ ml/min), $\overline{c}''_A = 0.343$ v/v, $R_C = 0.981$, and $R_{SC} = 11.2$. These operating conditions give $P = 0.992$, $R = 0.980$ when $c''_A = (1-\hat{\sigma}_A)\overline{c}''_A$ and $P = 0.980$, $R = 9.980$ when $c''_A = (1+\hat{\sigma}_A)\overline{c}''_A$.

As expected, robust operation is achieved at the expense of reducing the feed throughput ($\overline{Q}_F$ decreases from 1.21 to 0.507) and increasing solvent consumption (R_{SC} increases from 4.70 to 11.2). However, the actual loss in separation performance, 58% reduction in $\overline{Q}_F$ and 138% increase in R_{SC}, is much larger than might be anticipated for a

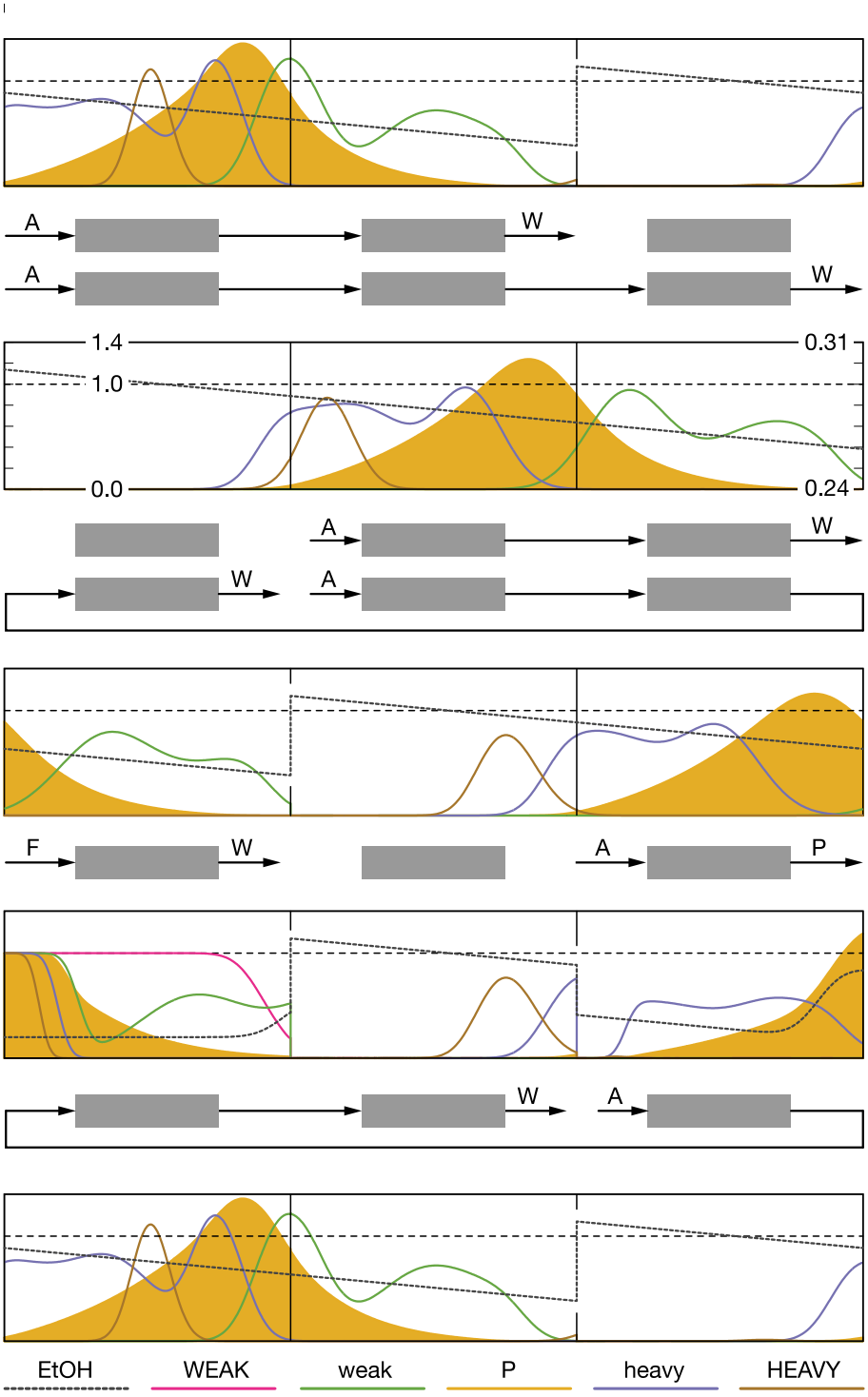

Fig. 6. Axial concentration profiles (c_i/c_i^F) in liquid phase under cyclic steady-state conditions for a GSSR cycle similar to the last one given in Table 2 but optimized for $c^F = 0.23$. Each solute concentration (c_i) is scaled by its value in the feed (c_i^F) and is read on the left y-axis. The dashed horizontal line represents the dimensionless feed concentration. The EtOH volume fraction is read on the right y-axis. The time instants at which the profiles are reported are from top to bottom: initial of the cycle, after one and two switch intervals, after the feed step, at the end of the cycle.

confidence interval of ±2%. This shows that the optimal conditions for nominal operation are not robust at all, and that the process must be operated very conservatively in order to withstand a 2% disturbance in c_A''. This level of flow rate accuracy is what is expected for a standard preparative HPLC pump, but dosing HPLC pumps can have flow rate accuracies as low as ±0.1%. But whatever the value of σ_A, the robust operating point provided by our approach is optimal, since it is the one that yields the best separation performance for the specified uncertainty.

Finally, and given that the best optimization reported in Table 2 gives $w_D = 0$, we examine the possibility of eliminating altogether the desorption zone while keeping the solvent consumption to a minimum. Thus, we keep $Q_A = 5.7$ ml/min, fix $Q_B = Q_C = 0$ ml/min, and from the superstructure given by Figs. 1 and 2 extract the cycle defined by

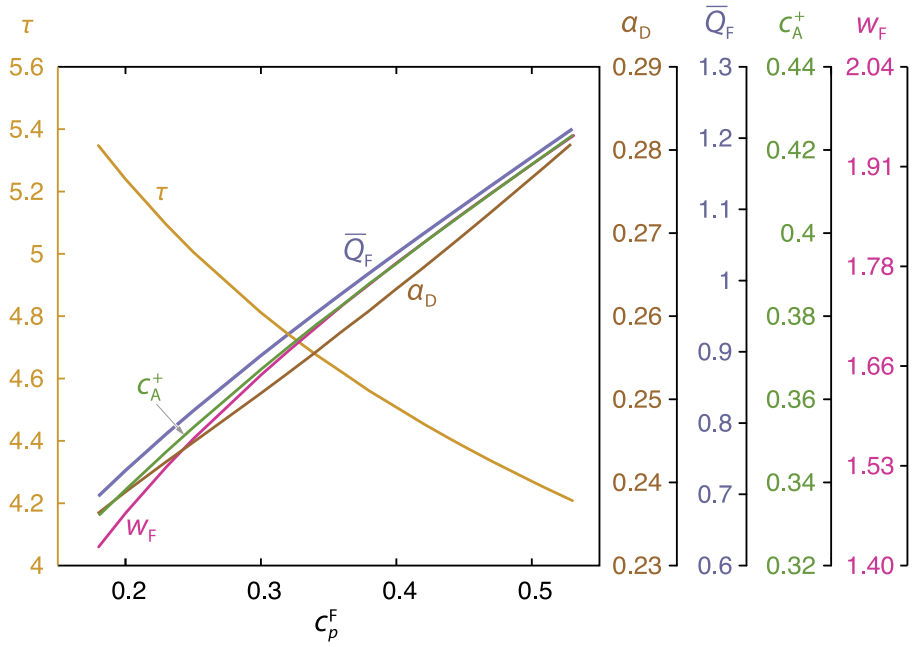

Fig. 7. Influence of the concentration of the target component in the feed, c_p^F, on the main parameters of the optimal GSSR purification cycle for $P_{min} = R_{min} = 0.98$ and fixed concentrations of the impurities in the feed.

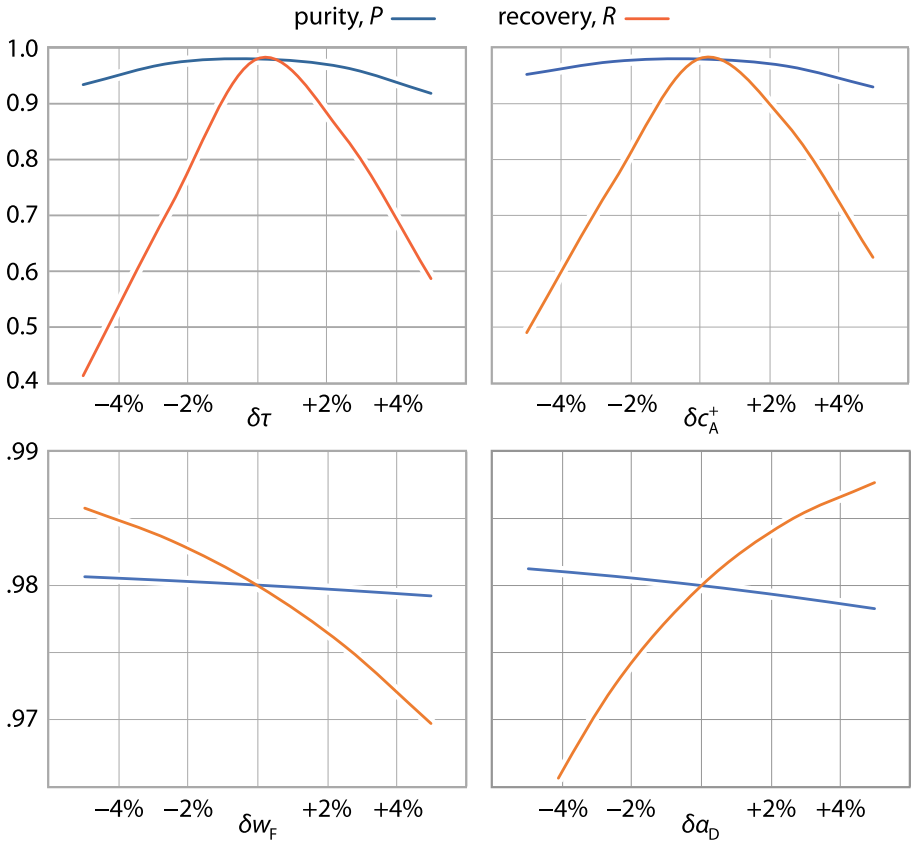

Fig. 8. Changes in purity (P) and recovery (R) as the following operating parameters are moved away from their optimal values: switching time, τ; volume of feed injected per cycle, w_F; end value of the periodic solvent gradient, c_A''; fraction of the switching interval allocated to the desorption step, α_D. For example, $\delta\tau = +2\%$ (−2%) means that τ is 2% larger (smaller) than its optimum value.

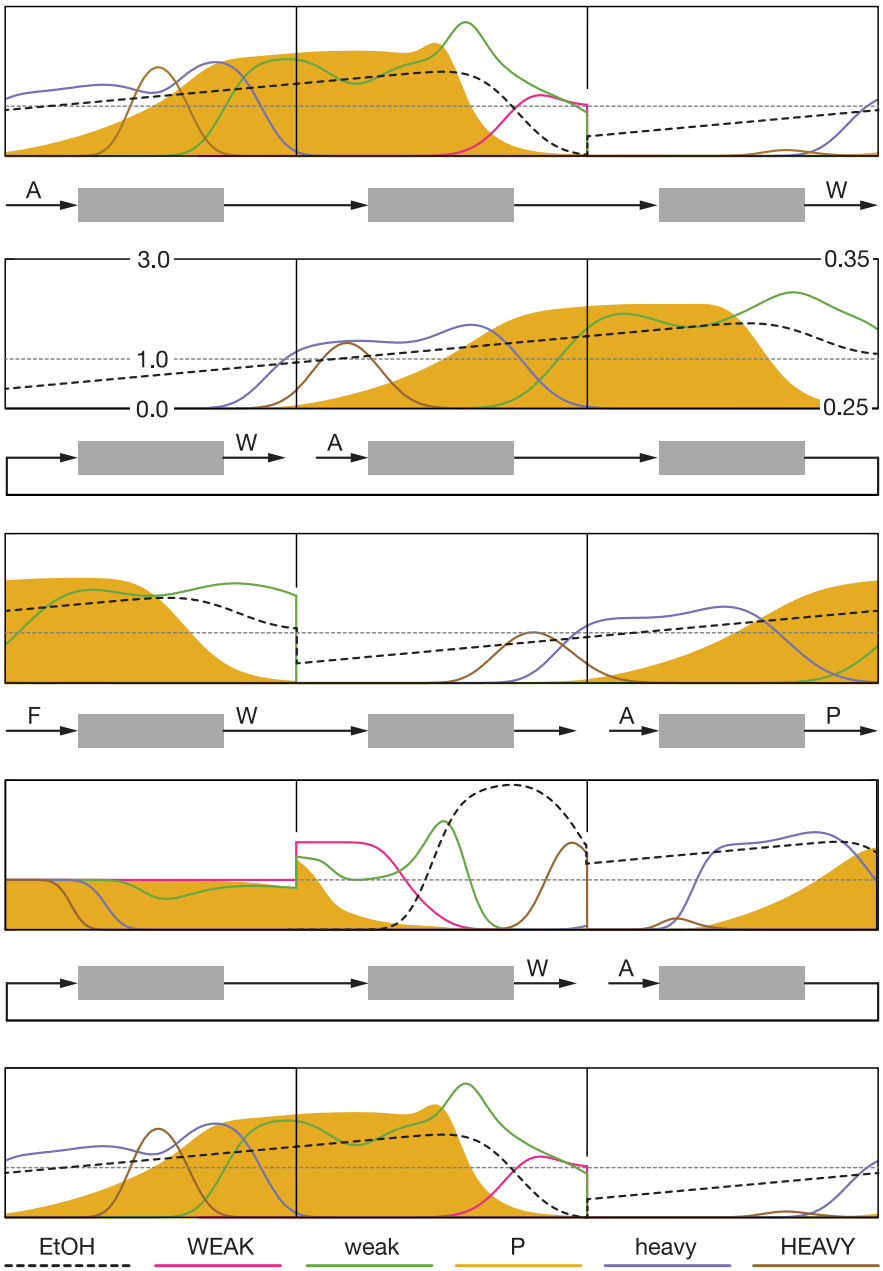

Fig. 9. Axial concentration profiles (c_i/c_i^{F}) in liquid phase under cyclic steady-state conditions for the optimization of the cycle defined by Eq. (36). Each solute concentration (c_i) is scaled by its value in the feed (c_i^{F}) and is read on the left y-axis. The dashed horizontal line represents the dimensionless feed concentration. The EtOH volume fraction is read on the right y-axis. The time instants at which the profiles are reported are from top to bottom: initial of the cycle, after one and two SWS, after the feed step, at the end of the cycle.

the following matrix S:

$$S = \begin{array}{c} (k,j) \\ 1 \\ 2 \\ 3 \\ 4 \end{array} \begin{array}{c} \begin{array}{ccc} 1 & 2 & 3 \end{array} \\ \begin{bmatrix} \mathrm{A} & \mathrm{O} & \mathrm{O} \\ \mathrm{O} & \mathrm{A} & \mathrm{O} \\ \mathrm{F} & \mathrm{O} & \mathrm{A} \\ \mathrm{O} & \mathrm{O} & \mathrm{A} \end{bmatrix} \end{array} \quad \begin{array}{l} \mathrm{A}\rightarrow\blacksquare\rightarrow\blacksquare\rightarrow\blacksquare\rightarrow \\ \quad\blacksquare\rightarrow\ \mathrm{A}\rightarrow\blacksquare\rightarrow\blacksquare\rightarrow\ \text{⌟} \\ \mathrm{F}\rightarrow\blacksquare\rightarrow\blacksquare\rightarrow\ \mathrm{A}\rightarrow\blacksquare\rightarrow\ \mathrm{P} \\ \quad\blacksquare\rightarrow\blacksquare\rightarrow\ \mathrm{A}\rightarrow\blacksquare\rightarrow\ \text{⌟} \end{array}, \tag{36}$$

where, as before, k runs over the set of steps, j the set of columns, and ⊏→ ⌟ means that the effluent at the downstream end of the system is recirculated back to the upstream end. The first two steps, each with duration τ, correspond to the first two SWS of the cycle, while the last two steps are the splitting of the third SW to accommodate the injection of feed and collection of product. Feed is injected at the upstream end of the system while product is collected at the downstream end during a fraction α_{P} of the SW. The normal operation of the column train is resumed during the last $(1-\alpha_{\mathrm{P}})\tau$ time units of the cycle.

The optimal operating conditions for this cycle, subject to the constraints $P_{\min} = R_{\min} = 0.98$ and $Q_{\mathrm{F}} \leq 10$ ml/min, are $\tau = 4.57$ min, $\alpha_{\mathrm{P}} = 0.370$, $w_{\mathrm{F}} = 2.15$ ($\overline{Q}_{\mathrm{F}} = 1.23$ ml/min), $c'_{\mathrm{A}} = 0.312$ v/v, $c''_{\mathrm{A}} = 0.263$ v/v, $R_{\mathrm{C}} = 1.72$, and $R_{\mathrm{SC}} = 4.19$. This solution is at least as good as the best one reported in Table 2, but with the added advantage of the cycle being somewhat simpler to implement experimentally. Interestingly, although the average modifier concentration in solvent A is approximately the same as those for the optimizations reported in Table 2, the slope of the modifier gradient is now negative and shallower. This set of results illustrates the potential of using advanced mathematical programming tools in designing and optimizing this type of processes for which it is very difficult to deduce sufficiently general heuristic rules.

Fig. 9 shows the optimized GSSR cycle along with snapshots of the axial concentration profiles in the three columns taken at the instants when switching between steps. It is seen that the system is more loaded with the target solute than in Figs. 5 and 6. While in the cycles in Figs. 5 and 6 the eluate from the column being injected with feed is discarded as waste, in the present case the eluate is directed to the next column. This allows more feed to be injected per cycle.

For the GSSR cycle depicted in Fig. 9, we reexamine its optimal robust design under uncertainty or variability in the operation of solvent gradient A from a slightly different perspective. Suppose that gradient A is generated by admixing the effluents of two isocratic pumps: one (pump A1) pumping solvent with EtOH concentration $c_{A1} = 0.25$ v/v and the other (pump A2) with EtOH concentration $c_{A2} = 0.5$ v/v. It is assumed that the pump motors have a small inertia of $\tau_A = 1$ s and the pumps a flow rate accuracy not exceeding $\hat{\sigma}_{A1} = \hat{\sigma}_{A2} = 1\%$.

If Q_A^* is the desired flow rate of solvent A and $c_A^*(t)$ the desired instantaneous EtOH concentration in gradient A, the set-points, Q_{A1}^* and Q_{A2}^*, for the flow rates of the two pumps are given by

$$Q_{A1}^*(t) = Q_A^* \frac{c_{A2}^* - c_A^*(t)}{c_{A2}^* - c_{A1}^*}, \quad Q_{A2}^*(t) = Q_A^* \frac{c_A^*(t) - c_{A1}^*}{c_{A2}^* - c_{A1}^*}. \tag{37}$$

But due to the limited accuracy of the pumps and small inertia of their motors, the actual flow rates, Q_{A1} and Q_{A2}, are not exactly equal to their set-points, but governed by first-order dynamics with set-point uncertainty:

$$\tau_A \frac{dQ_{A1}}{dt} = (1+\sigma_{A1})Q_{A1}^* - Q_{A1}, \quad \tau_A \frac{dQ_{A2}}{dt} = (1+\sigma_{A2})Q_{A2}^* - Q_{A2}, \tag{38}$$

where $-\hat{\sigma}_{A1} \le \sigma_{A1} \le +\hat{\sigma}_{A1}$ and $-\hat{\sigma}_{A2} \le \sigma_{A2} \le +\hat{\sigma}_{A2}$ are the actual deviations (as fraction of the operating flow rate) within the uncertainty range. Obviously, if $\tau_A = 0$ then there will be no lag in the response of the pumps, but they will only deliver exactly the desired flow rate for $\sigma_{A1} = \sigma_{A2} = 0$.

Fig. 10 shows the effect of the 1 s inertia and flow rate accuracy of ±1% of pumps A1 and A2 on the steady periodic EtOH gradient profile. The profile is plotted over two SWS. The solid curves correspond to the four vertices of the uncertainty region of flow rate accuracy on the $\sigma_{A1} \times \sigma_{A2}$ plane: $(-0.01, -0, 01)$, $(-0.01, +0, 01)$, $(+0.01, -0, 01)$, $(+0.01, +0, 01)$. The dashed lines represent the desired profile. In the absence of the effect of inertia, Q_A^* would be bounded by the profiles generated by the vertices of the uncertainty region of flow rate accuracy, but $c_A(t)$ would not. However, as discussed above the important variable is the product $Q_A c_A \tau$ and not Q_A or c_A alone, and Fig. 10 shows that $Q_A c_A$ lies within the region delimited by the two vertices $(-0.01, -0.01)$ and $(+0.01, +0, 01)$ of the uncertainty region.

Using the same approach as before, the optimal operating conditions when c_A'' is subject to the uncertainty given by Eq. (38) can be determined by solving the following robust NLP problem:

$$\max_{\mathcal{V}} \ \overline{Q}_F \tag{39}$$

$$\text{s.t. } c^- = h^{CSS}(\mathcal{V}, \mathcal{P}, 1-\hat{\sigma}_{A1}, 1-\hat{\sigma}_{A2}), \tag{40}$$

$$c^+ = h^{CSS}(\mathcal{V}, \mathcal{P}, 1+\hat{\sigma}_{A1}, 1+\hat{\sigma}_{A2}), \tag{41}$$

$$P^- \equiv P(c^-, \mathcal{V}, \mathcal{P}) \ge P_{min}, \quad P^+ \equiv P(c^+, \mathcal{V}, \mathcal{P}) \ge P_{min}, \tag{42}$$

$$R^- \equiv R(c^-, \mathcal{V}, \mathcal{P}) \ge R_{min}, \quad R^+ \equiv R(c^+, \mathcal{V}, \mathcal{P}) \ge R_{min}, \tag{43}$$

where $\mathcal{V} = \{\tau, \alpha_D, w_F, c_A', c_A''\}$ is the set of design or decision variables.

The optimal robust operating conditions, subject to the constraints $\hat{\sigma}_{A1} = \hat{\sigma}_{A2} = 0.01$, $P_{min} = R_{min} = 0.98$, and $Q_F \le 10$ ml/min, are $\tau = 4.75$ min, $\alpha_P = 0.376$, $w_F = 1.84$ ($\overline{Q}_F = 1.02$ ml/min and $Q_F = 8.12$ ml/min), $c_A' = 0.314$ v/v, $c_A'' = 0.250$ v/v. The purity, recovery, and KPI values for the two worst cases are $P^- = 0.984$, $R^- = 0.980$, $R_C^- = 1.41$, $P^+ = 0.980$, $R^+ = 0.980$, $R_C^+ = 1.38$. When $\sigma_{A1} = \sigma_{A2} = -0.01$ the flow rate of solvent A is $Q_A^- = 5.64$ ml/min and $R_{SC}^- = 5.55$; when $\sigma_{A1} = \sigma_{A2} = +0.01$ it is $Q_A^+ = 5.76$ ml/min and $R_{SC}^+ = 5.66$. As before, robust operation is achieved at the expense of reducing the productivity ($\overline{Q}_F$ decreases from 1.23 ml/min to 1.02 ml/min) and increasing the solvent consumption (R_{SC} increases from 4.19 to ~ 5.6). However, in this case the actual loss in separation performance is nowhere near as bad as in the previously examined case.

7. Conclusions

One instance of GSSR chromatography for peptide purification has been optimized using state-of-the-art mathematical programming tools. The optimization problem was formulated using a full-discretization approach for steady periodic dynamics and the resulting nonlinear programming problem solved by an efficient open-source interior-point solver coupled to a high-performance parallel linear solver for sparse symmetric indefinite matrices.

This procedure was successfully employed to find optimal solutions for a series of process design problems with increasing number of decision variables. In addition to productivity and recovery, process performance was analyzed in terms of two key performance indicators: dilution ratio and solvent consumption ratio.

Finally, the problem of robust process design under uncertainty of manipulating the solvent gradient was examined. The best solution is chosen only among candidate solutions that are robust feasible, that is, remain feasible for all modifier gradient perturbations within the accuracy of the gradient pump. This gives rise to a robust approach to optimal design in which the nominal problem is replaced by a worst case problem.

In one case the upper boundary of the solvent gradient is subject to uncertainty which nonetheless is bounded by known lower and upper limits. In a second case it is assumed that the two HPLC pump motors that generate the solvent gradient have a small inertia and a flow rate accuracy not exceeding a given known value. As expected, robust operation is achieved at the expense of reducing the feed throughput and increasing solvent consumption. Still, the robust operating point provided by our approach is optimal, since it is the one that yields the best separation performance for the specified uncertainty.

Overall, our work illustrates the advantages of using advanced mathematical programming tools in designing and optimizing this type of processes for which it is very difficult to deduce sufficiently general heuristic design rules.

Funding

The authors acknowledge the financial support from the Portuguese Foundation for Science and Technology (FCT/MCTES) through PhD grants BD/142951/2018 (T.P.D. Santos) and BD/06003/2020 (R.P. Fernandes). This research was partly supported by the Associate Laboratory for Green Chemistry-LAQV, which is financed by national funds from FCT/MCTES (UIDB/50006/2020 and UIDP/50006/2020).

Declaration of competing interest

The authors declare that they have no known competing financial interests or personal relationships that could have appeared to influence the work reported in this paper.

Data availability

Data will be made available on request.

Appendix A. Supplementary data

Supplementary material related to this article can be found online at https://doi.org/10.1016/j.dche.2022.100081.

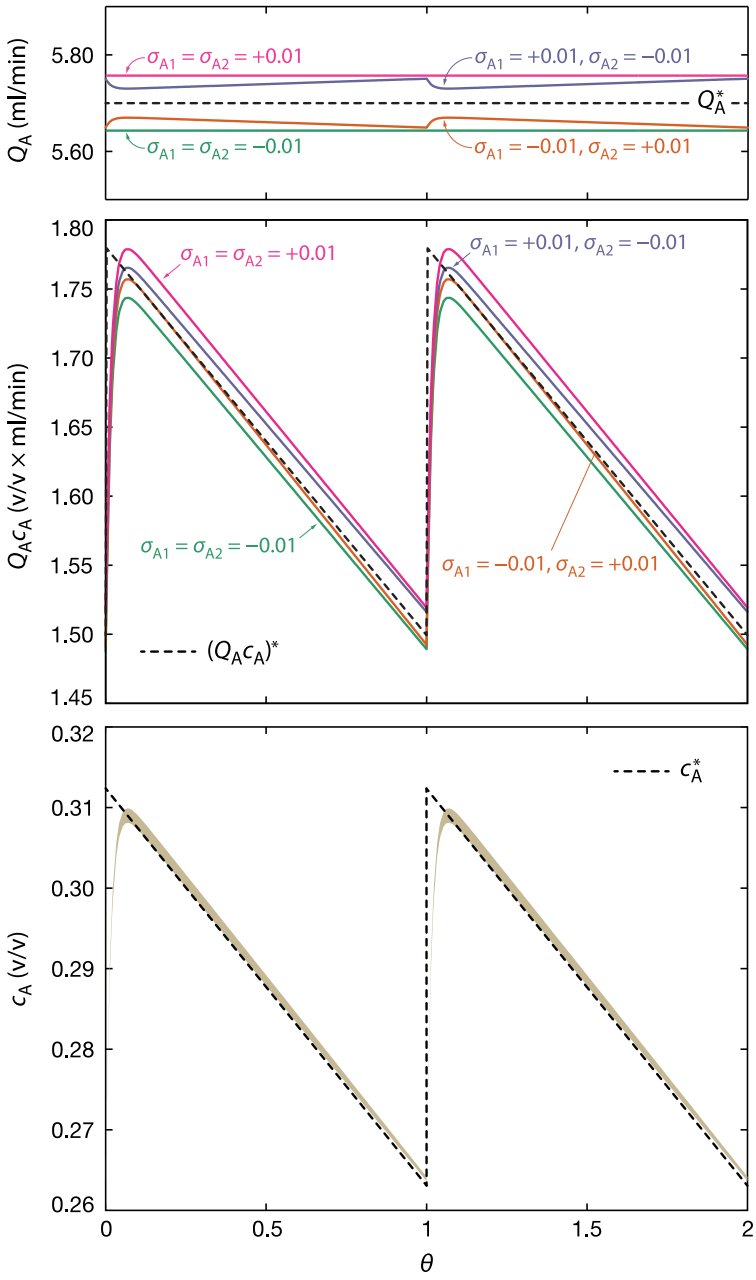

Fig. 10. Effect of inertia ($\tau_A = 1$ s) and flow rate accuracy ($\sigma_A = \sigma_{A1} = \sigma_{A2}$) of pumps A1 and A2 on the steady periodic EtOH gradient profile. The profile is plotted over two consecutive sws. The solid curves correspond to the four vertices of the uncertainty region of flow rate accuracy on the $(\sigma_{A1}, \sigma_{A2})$ plane: $(-0.01, -0, 01)$, $(-0.01, +0, 01)$, $(+0.01, -0, 01)$, $(+0.01, +0, 01)$. The dashed lines represent the desired profile.

References

Abbood, A., Smadja, C., Herrenknecht, C., Alahmad, Y., Tchapla, A., Taverna, M., 2009. Retention mechanism of peptides on a stationary phase embedded with a quaternary ammonium group: A liquid chromatography study. J. Chromatogr. A 1216, 3244–3251.

AMPL, 2022. https://ampl.com/. (Accessed 13 October 2022).

Angarita, M., Müller-Späth, T., Baur, D., Lievrouw, R., Lissens, G., Morbidelli, M., 2015. Twin-column CaptureSMB: A novel cyclic process for protein a affinity chromatography. J. Chromatogr. A 1389, 85–95.

Anon, 2021. Watson Sparse Matrix Package (WSMP) - IBM research. https://researcher.watson.ibm.com/researcher/view_group.php?id=1426. (Accessed on 13 October 2022).

Araújo, J.M.M., Rodrigues, R.C.R., Mota, J.P.B., 2006. Optimal design and operation of a certain class of asynchronous simulated moving bed processes. J. Chromatogr. 1132 (1–2), 76–89.

Aumann, L., Morbidelli, M., 2007. A continuous multicolumn countercurrent solvent gradient purification (MCSGP) process. Biotechnol. Bioeng. 98 (5), 1043–1055.

Aumann, L., Morbidelli, M., 2008. A semicontinuous 3-column countercurrent solvent gradient purification (MCSGP) process. Biotechnol. Bioeng. 99, 728–733.

Aumann, L., Ströhlein, G., Morbidelli, M., 2007. Parametric study of a 6-column countercurrent solvent gradient purification (MCSGP) unit. Biotechnol. Bioeng. 98, 1029–1042.

Baur, D., Angarita, D.M., Müller-Späth, T., Steinebach, F., Morbidelli, M., 2016. Comparison of batch and continuous multi-column protein a capture processes by optimal design. Biotechnol. J. 11 (7), 920–993.

Brämer, C., Lammers, F., Scheper, T., Beutel, S., 2019. Development and testing of a 4-columns periodic counter-current chromatography system based on membrane adsorbers. Separations 6 (4), 55.

Challener, C.A., 2018. Making the move to continuous chromatography. BioPharm Int. 31 (4), 14–18, 2018.

COIN-OR, 2022. Interior Point Optimizer - IPOPT. https://github.com/coin-or/Ipopt/. (Accessed on 13 October 2022).

De Luca, C., Felletti, S., Lievore, G., Buratti, A., Cavazzini, A., Catania, M., Spon-chioni, M., Macis, M., Ricci, A., Cabri, W., 2020. Boosting the purification process of biopharmaceuticals by means of continuous chromatography. LCGC 6 (38), 30–34.

Godawat, R., Brower, K., Jain, S., Konstantinov, K., Riske, F., Warikoo, V., 2012. Periodic counter-current chromatography – Design and operational considerations for integrated and continuous purification of proteins. Biotechnol. J. 7 (12), 1496–1508.

Gomis-Fons, J., Andersson, N., Nilsson, B., 2020. Optimization study on periodic counter-current chromatography integrated in a monoclonal antibody downstream process. J. Chromatogr. A 1621, 461055.

Guiochon, G., Felinger, A., Shirazi, D.G., Katti, A.M., 2006. Fundamentals of Preparative and Nonlinear Chromatography, second ed. Elsevier, San Diego.

Gupta, A., 2000. WSMP: Watson Sparse Matrix Package (Part I - Direct Solution of Symmetric Sparse Systems). Technical Report RC 21886, IBM T. J. Watson Research Center, Yorktown Heights, NY, 2000.

Holzer, M., Osuna-Sanchez, H., David, L., 2008. Multicolumn chromatography. BioProcess Int. 6 (8), 74.

Hur, J.S., Wankat, P.C., 2005. New design of simulated moving bed (SMB) for ternary separations. Ind. Eng. Chem. Res. 44 (6), 1906–1913.

Kawajiri, Y., 2021. Model-based optimization strategies for chromatographic processes: A review. Adsorption 27, 1–26.

Kumar, V., Rathore, A.S., 2014. Two-stage chromatographic separation of aggregates for monoclonal antibody therapeutics. J. Chromatogr. A 1368, 155–162.

Lee, J.W., 2020. Expanding simulated moving bed chromatography into ternary separations in analogy to dividing wall column distillation. Ind. Eng. Chem. Res. 59 (20), 9619–9628.

Lin, D.-Q., Zhang, Q.-L., Yao, S.-J., 2021. Model-assisted approaches for continuous chromatography: Current situation and challenges. J. Chromatogr. A 1637, 461855.

Ludemann-Hombourger, O., Nicoud, R.M., Bailly, M., 2000. The varicol process: A new multicolumn continuous chromatographic process. Sep. Sci. Technol. 35 (12), 1829–1862.

Mahajan, E., George, A., Wolk, B., 2012. Improving affinity chromatography resin efficiency using semi-continuous chromatography. J. Chromatogr. A 1227, 154–162.

Mota, J.P.B., Araújo, J.M.M., Rodrigues, R.C.R., 2007a. Optimal design of simulated moving-bed processes under flow rate uncertainty. AIChE J. 53 (10), 2630–2642.

Mota, J.P.B., Esteves, I.A.A.C., Euseébio, M.F.J., 2007b. Synchronous and asynchronous SMB processes for gas separation. AIChE J. 53 (5), 1192–1203.

Müller-Späth, T., Aumann, L., Melter, L., Strölein, G., Morbidelli, M., 2008. Chromatographic separation of three monoclonal antibody variants using multicolumn countercurrent solvent gradient purification (MCSGP). Biotechnol. Bioeng. 100 (1166).

Nestola, P., Peixoto, C., Silva, R.R.J.S., Alves, P.M., Carrondo, J.M.T., Mota, J.P.B., 2015. Robust design of adenovirus purification by two-column, simulated moving-bed, size-exclusion chromatography. J. Biotechnol. 213, 109–119.

OpenBLAS, 2022. OpenBLAS: An optimized BLAS library. https://www.openblas.net. (Accessed on 13 October 2022).

Pagkaliwangan, M., Hummel, J., Gjoka, X., Bisschops, M., Schofield, M., 2019. Optimized continuous multicolumn chromatography enables increased productivities and cost savings by employing more columns. Biotech. J. 14, 1800179.

Pollock, J., Coffman, J., Ho, S.V., Farid, S.S., 2017. Integrated continuous bioprocessing: Economic, operational, and environmental feasibility for clinical and commercial antibody manufacture. Biotechnol. Progr. 33 (4), 854–866.

Rodrigues, R.C.R., Araújo, J.M.M., Euseébio, M.F.J., Mota, J.P.B., 2007a. Experimental assessment of simulated moving bed and varicol processes using a single-column setup. J. Chromatogr. A 1142 (1), 69–80.

Rodrigues, R.C.R., Araújo, J.M.M., Mota, J.P.B., 2007b. Optimal design and experimental validation of synchronous, asynchronous and flow-modulated, simulated moving-bed processes using a single-column setup. J. Chromatogr. A 1162 (1), 14–23.

Ruthven, D.M., 1984. Principles of Adsorption and Adsorption Processes. John Wiley & Sons, New York.

Schmölder, J., Kaspereit, M., 2020. A modular framework for the modelling and optimization of advanced chromatographic processes. Processes 8 (1), 65.

Shi, C., Gao, Z.-Y., Zhang, Q.-L., Yao, S.-J., Slater, N.K.H., Lin, D.-Q., 2020. Model-based process development of continuous chromatography for antibody capture: A case study with twin-column system. J. Chromatogr. A 1619, 460936.

Silva, R.J.S., Rodrigues, R.C.R., Mota, J.P.B., 2012. Relay simulated moving bed chromatography: Concept and design criteria. J. Chromatogr. A 1260, 132–142.

Silva, R.J.S., Rodrigues, R.C.R., Osuna-Sanchez, H., Bailly, M., Valéry, E., Mota, J.P.B., 2010. A new multicolumn, open-loop process for center-cut separation by solvent-gradient chromatography. J. Chromatogr. A 1217 (52), 8257–8269.

Sreedhar, B., Kawajiri, Y., 2014. Multi-column chromatographic process development using simulated moving bed superstructure and simultaneous optimization – Model correction framework. Chem. Eng. Sci. 116, 428–441.

Steinebach, F., Ulmer, N., Decker, L., Aumann, L., Morbidelli, M., 2017. Experimental design of a twin-column countercurrent gradient purification process. J. Chromatogr. A 1492, 19–26.

Ströhlein, G., Aumann, L., Mazzotti, M., Morbidelli, M., 2006. A continuous, countercurrent multi-column chromatographic process incorporating modifier gradients for ternary separations. J. Chromatogr. A 1126 (1), 338–346.

Wächter, A., Biegler, L.T., 2006. On the implementation of an interior-point filter line-search algorithm for large-scale nonlinear programming. Math. Program. Ser. A 106, 25–57.

Warikoo, V., Godawat, R., Brower, K., Jain, S., Cummings, D., Simons, E., Johnson, T., Walther, J., Yu, M., Wright, B., McLarty, J., Karey, K.P., Hwang, C., Zhou, W., Riske, F., Konstantinov, K., 2012. Integrated continuous production of recombinant therapeutic proteins. Biotech. Bioeng. 109 (12), 3018–3029.